

From Stellar Coronæ to Gyrochronology: a theoretical and observational exploration

J. Ahuir, A. S. Brun and A. Strugarek

Département d'Astrophysique-AIM, CEA/DRF/IRFU, CNRS/INSU, Université Paris-Saclay, Université Paris-Diderot, Université de Paris, F-91191 Gif-sur-Yvette, France
e-mail: jeremy.ahuir@cea.fr

Received XXX ; accepted YYY

ABSTRACT

Context. Stellar spin-down is the result of a complex process involving rotation, dynamo, wind and magnetism. Multi-wavelength surveys of solar-like stars have revealed the likely existence of relationships between their rotation, X-ray luminosity, mass-losses and magnetism. Those impose strong constraints on the corona and wind of cool stars.

Aims. We aim to provide power-law prescriptions of the mass-loss of stars, of their magnetic field, and of their base coronal density and temperature that are compatible with their observationally-constrained spin-down.

Methods. We link the magnetic field and the mass-loss rate from a wind torque formulation in agreement with the distribution of stellar rotation periods in open clusters and the Skumanich law. Given a wind model and an expression of the X-ray luminosity from radiative losses, we constrain the coronal properties by assuming different physical scenarii linking closed loops to coronal holes.

Results. We find that the magnetic field and the mass loss are involved in a one-to-one correspondence constrained from spin-down considerations. We show that a magnetic field depending on both the Rossby number and the stellar mass is required to keep a consistent spin-down model. The estimates of the magnetic field and the mass-loss rate obtained from our formalism are consistent with statistical studies as well as individual observations and give new leads to constrain the magnetic field-rotation relation. The set of scaling-laws we derived can be broadly applied to cool stars from the PMS to the end of the MS, and allow for a stellar wind modelling consistent with all the observational constraints available to date.

Key words. stars: rotation – stars: magnetic fields – stars: mass-loss – stars: winds, outflows – stars: solar-type

1. Introduction

The rotation of stars is subject to a complex evolution along their life. During the early stage of their lifetime, solar-type stars spin-up as they contract during the Pre-Main Sequence. Once the Zero-Age Main Sequence (ZAMS) is reached, they keep their moment of inertia relatively constant (Armitage & Clarke 1996) while they lose mass and angular momentum through the flow of a magnetized stellar wind (Schatzman 1962; Weber & Davis 1967; Mestel 1968). It results in a slow-down of their rotation as they age, which approximately follows the empirical Skumanich's law: $\Omega_{\star} \propto t^{-0.5}$ (Skumanich 1972). This spin-down also depends on the stellar mass (Weber & Davis 1967; Matt et al. 2015). Indeed, during most of the Pre-Main Sequence, lower mass stars tend to remain fast rotators for a longer time than the higher mass stars. Then, after hundreds of millions of years, the slowest rotators converge toward a sequence in which the rotation rate increases with mass. These phenomena make gyrochronology possible (Barnes 2003), thereby allowing the estimation of stellar ages through measurements of rotation periods and masses.

Understanding the feedback loop between rotation, dynamo action, magnetism and wind is a key issue to predict the behavior of the solar-like stars as they evolve. It is also important to understand the evolution of star-planet systems and to follow potential planetary migrations (Zhang & Penev 2014; Benbakoura et al. 2019). Our ability to track the stellar rotation evolution strongly relies on the wind braking modeling. Most angular momentum

evolution models fall back on the Kawaler (1988) prescription to assess the wind torque, which is expressed in this model as a power-law depending on the magnetic field, the mass-loss rate, the mass and the radius of the star. Several modifications have since been brought to this formulation (Krishnamurthi et al. 1997; Bouvier et al. 1997; Reiners & Mohanty 2012). For instance, to account for fast rotators on the ZAMS, a saturation of the braking torque is required (Barnes & Sofia 1996). Magneto-hydrodynamical simulations can also be used to assess of the angular momentum loss due to the wind. For instance, Matt et al. (2012), following Matt & Pudritz (2008), simulated the flow of a stellar wind along the opened field lines of a dipolar configuration to estimate the torque, by taking into account the influence of stellar rotation on the wind acceleration (Sakurai 1985). More recently, modified versions of this formulation were presented to take into account the influence of the magnetic topology. Réville et al. (2015a) considered the magnetic flux through the open field lines to build a topology-independent wind torque, while Finley & Matt (2017, 2018) relied on a broken power-law behavior to deal with combined geometries. Garraffo et al. (2016, 2018) accounted for magnetic topology by means of a modulating factor to the angular momentum loss estimated for a dipolar configuration. In general, in most of the prescriptions of spin-evolution torques, it is assumed that the wind carries away angular momentum at a rate proportional to Ω_{\star}^3 during the Main Sequence in order to follow the Skumanich law. It is important to note that the Skumanich law is today questioned for evolved stars. Some recent studies have shown a substantial decrease of

the wind braking efficiency for evolved stars around the solar value of the Rossby number (van Saders et al. 2016), even if this alternative scenario seems to be in disagreement with solar twins studies (Lorenzo-Oliveira et al. 2019).

To estimate the angular momentum loss, we need to know accurately the stellar magnetic field and the properties of its wind (such as the mass loss induced). The latter are bound to physical parameters in the corona, like the plasma temperature and density. Several observational trends constrain and correlate those different quantities: the mass loss (Wood et al. 2002, 2005; Jardine & Collier Cameron 2019), the X-ray activity (Pizzolato et al. 2003; Wright et al. 2011; Reiners et al. 2014), the magnetic field (Vidotto et al. 2014; See et al. 2017) and the rotation rate of the star for different ages (Agüeros et al. 2011; McQuillan et al. 2014; Gallet & Bouvier 2015). Coupling all those quantities is therefore necessary to design a consistent model of stellar spin-down.

A preliminary exploration has been carried out by Blackman & Owen (2016), who presented a simplified model for the coupled time evolution of the relevant quantities on the basis of a pressure-driven isothermal wind (Parker 1958). In this framework, a dynamo-induced magnetic field dictates the behavior of the stellar wind and the X-ray luminosity through a coronal equilibrium. More recently, Skumanich (2019) focused on the connections between the physical parameters regulating the stellar spin-down by considering their rotational evolution. By assuming a direct correlation between the mass loss and the magnetic field, he studied the influence of the Skumanich law on all the relevant quantities by means on a variety of observational trends. Such a study suggest that the magnetic field and the rotation of cool star should scale linearly, while the mass-loss should scale quadratically with stellar rotation.

More generally, stellar wind models require the knowledge of the coronal temperature and density. To be consistent with the aforementioned correlations, one need to constrain those two quantities from tracers of the coronal activity, like the soft X-ray emission of the star. In this spirit, by relying on a 1D polytropic and magnetocentrifugal wind, Holzwarth & Jardine (2007) provided scaling laws in accordance with the rotational evolution of the X-ray luminosity (Ivanova & Taam 2003) and the empirical mass loss-X-ray flux correlation from Wood et al. (2005).

Building on those previous studies, the main goal of this paper is to infer from stellar spin-down considerations some prescriptions of the magnetic field, the mass loss, the coronal temperature and the coronal density as a function of fundamental stellar parameters (such as mass, radius and rotation rate) in order to be consistent with all the observational trends. Each of those constraints are successively introduced to eliminate the largest number of free parameters involved in the spin-down process. Please note that in our attempt to extract the most important interdependencies between various physical mechanisms involved in stellar spin down theory, we had to make some simplifying assumptions but we have been careful to retain all the key mechanisms. Our scaling laws provide a novel and systematic way to connect all these mechanisms together and should be seen as a first approach to systematically characterize these complex relationships between the stellar parameters. In Section 2 we introduce the theoretical framework we used for the torque parametrization. In Section 3 observational constraints are leveraged to unveil the inter-dependency of the magnetic field and the mass-loss rate of cool stars. We further derive the associated prescriptions for the coronal temperature and the coronal density for a given wind model. In Section 4, we summarize our prescrip-

tions and give a practical application to the case of ϵ Eridani. All those results are then summarized, discussed and put in perspective in Section 5.

2. Stellar wind torques of solar-type stars: theoretical approach

2.1. Fundamental stellar parameters and architecture of the model

First of all, designing a consistent model for the stellar spin-down requires to inventory the coupling between the various physical mechanisms (and their associated control parameters) involved in the process.

Stellar rotation and magnetism strengthen the supersonic flow of a stellar wind (Weber & Davis 1967), which entails itself a mass loss \dot{M} . The wind then carries away angular momentum, leading to a braking torque Γ_{wind} spinning down the star. The logical sequence from fundamental stellar parameters to the wind braking torque and the role of the X-ray luminosity inside the architecture of the model is summarized in Figure 1, where we show all the interdependencies between the various physical mechanisms and their control parameters. Theoretical assumptions are represented in blue and are essentially related to the wind torque parametrization, dynamo scalings as well as the choice of a wind model. Observational trends, in red, are taken as constraints for the physical models (see Appendix F for an extensive view of those ingredients and their caveats).

Solar-type stars generate a magnetic field through a dynamo in their envelope (Brun et al. 2004, 2015) triggered by turbulent convective movements. Those can be influenced by stellar rotation (Durney & Latour 1978). This effect can be quantified by the Rossby number Ro , which has been shown to be a relevant quantity to characterize the magnetic activity of the stars (Noyes et al. 1984). Direct spectropolarimetric studies also exhibit scaling laws linking the stellar magnetic field and this dimensionless number (Vidotto et al. 2014; See et al. 2017). However, multiple definitions of the Rossby number are available in the literature, which has forced the community to clarify this aspect (Landin et al. 2010; Brun et al. 2017; Amard et al. 2019). In this work, the Rossby number will be normalized to the solar value. This way, different prescriptions of the Rossby number can be equally used as long as they differ only by a proportionality factor. This is generally the case of main-sequence stars, which we will focus on here. However, to deal with individual stars, we will use for simplicity the stellar Rossby number, expressed as

$$Ro = \frac{P_{\text{rot}}}{\tau_c}, \quad (1)$$

with P_{rot} the stellar rotation period and τ_c the convective turnover time. The latter can itself be assessed at different locations or computed in a variety of ways, which are often linked to a given stellar evolution model (Landin et al. 2010; Cranmer & Saar 2011; Sadeghi Ardestani et al. 2017) or a set of observations (Wright et al. 2011).

Coronal activity, measured with the X-ray emission of the star, has been correlated with the stellar magnetic field (Petsov et al. 2003; Vidotto et al. 2014) and the mass loss (Wood et al. 2002, 2005). Observations have also exhibited a relationship between the stellar rotation and the X-ray luminosity for main sequence stars (Noyes et al. 1984; Pizzolato et al. 2003; Wright et al. 2011; Vidotto et al. 2014; Reiners et al. 2014), allowing us to link the coronal activity to fundamental stellar parameters.

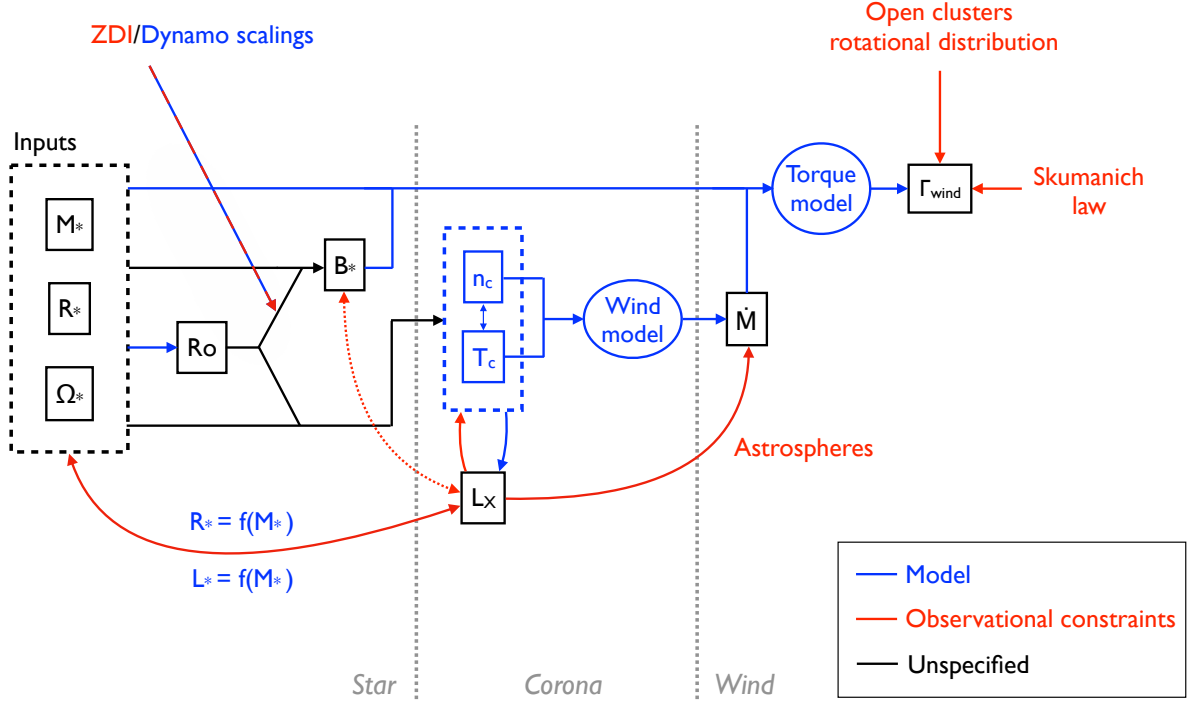


Fig. 1. Sketch of the multiple couplings between the inputs of the model (stellar mass, radius and rotation rate), the magnetic field, the X-ray luminosity, the coronal temperature and density, the mass loss and the wind braking torque. In blue: model assumptions. In red: observational constraints.

This gives us the opportunity to closely link those physical quantities together through stellar activity considerations.

Furthermore, the corona of the stars we consider is thought to be heated up through magnetic processes (for a review, see Mathioudakis et al. 2013; Cranmer, Gibson & Riley 2017) to reach a typical coronal temperature T_c of around 10^6 K (Suzuki & Inutsuka 2006). Such a hot and diluted medium (with a density n_c) expands and generates a transsonic wind (Parker 1958). Observationally, scaling laws have been established between the coronal temperature and the X-ray emission of the star (Preibisch 1997; Johnstone & Güdel 2015; Wood et al. 2018). From a theoretical point of view, the latter can be deduced from coronal properties by estimating the radiative losses in the X-ray-emitting area of the corona (Ivanova & Taam 2003; Aschwanden 2004; Blackman & Owen 2016). Therefore, it could be possible to provide a prescription for the coronal temperature and density in terms of stellar mass, radius and rotation rate.

2.2. Torque parametrization

Solar-like stars spin down due to the angular momentum extraction by the stellar wind (Schatzman 1962). Weber & Davis (1967) showed with a 1D model in the stellar equatorial plane that the angular momentum loss Γ_{wind} can be estimated at the Alfvén radius r_A as

$$\Gamma_{\text{wind}} = \dot{M} r_A^2 \Omega_\star, \quad (2)$$

with Ω_\star the stellar rotation rate and \dot{M} the mass loss. The Alfvén radius can be expressed as a function of the stellar magnetic field, the mass loss and other fundamental stellar parameters, such as the stellar mass, the stellar radius and the stellar rotation rate (Kawaler 1988). For instance, Matt et al. (2012) presented the following expression for this characteristic distance, by assum-

ing a dipolar magnetic field:

$$\frac{\langle r_A \rangle}{R_\star} = K_1 \left[\frac{\Upsilon}{\sqrt{K_2^2 + 0.5f^2}} \right]^m, \quad (3)$$

where M_\star is the stellar mass, R_\star the stellar radius, K_1 , K_2 and m are constants set using 2D MHD simulations. More precisely, K_1 is used to calibrate the solar wind torque, K_2 the efficiency of the magnetocentrifugal acceleration (Sakurai 1985), and m stands for a magnetic topology parameter (Réville et al. 2015a). For a dipolar field, we will use the value proposed in Matt et al.

(2012), *i.e.* $m = 0.2177$. $f = \Omega_\star / \sqrt{GM_\star/R_\star^3}$ is the break-up ratio, obtained by dividing the stellar rotation rate at the equator of the star by the keplerian angular velocity. The magnetization parameter Υ (Matt & Pudritz 2008) is defined as

$$\Upsilon = \frac{B_\star^2 R_\star^2}{\dot{M} v_{\text{esc}}}, \quad (4)$$

with B_\star the magnetic field strength at the stellar equator and $v_{\text{esc}} = \sqrt{2GM_\star/R_\star}$ the escape velocity. With this formulation, the wind braking torque becomes

$$\begin{aligned} \Gamma_{\text{wind}} &= \dot{M} \Omega_\star R_\star^2 K_1^2 \left[\frac{\Upsilon}{\sqrt{K_2^2 + 0.5f^2}} \right]^{2m} \\ &\propto \dot{M}^{1-2m} B_\star^{4m} R_\star^{2+5m} M_\star^{-m} \Omega_\star (K_2^2 + 0.5f^2)^{-m}. \end{aligned} \quad (5)$$

We will rewrite this power-law expansion of the torque to adopt the following generic expression

$$\Gamma_{\text{wind}} \propto \dot{M}^{1-2m} B_\star^{4m} R_\star^{2+5m} M_\star^{-m} \Omega_\star \left[1 + \frac{f^2}{K^2} \right]^{-m}, \quad (6)$$

where $K = \sqrt{2}K_2$ is a constant.

2.3. Stellar magnetic field prescription

Computing the wind braking torque requires to estimate the stellar magnetic field and the mass-loss rate. We focus here on the surface magnetic field strength at the stellar equator B_\star . For the sake of simplicity we will assume a power-law expression for the magnetic field as a function of the stellar mass, the stellar radius and the Rossby number as

$$B_\star \propto \left(\frac{Ro}{Ro_\odot}\right)^{-p_B} \left(\frac{R_\star}{R_\odot}\right)^{r_B} \left(\frac{M_\star}{M_\odot}\right)^{m_B}, \quad (7)$$

where p_B, m_B & r_B are unspecified exponents for the time being.

Since we will present in the remaining of this work a significant number of power-law prescriptions, we have to fix a generic notation for the different exponents. More precisely, for the physical quantities we want to estimate (namely the magnetic field, the mass loss and the coronal properties), we will write a given exponent with a lowercase letter indicating the variable of the power law (p for the rotation period, r for the stellar radius and m for the stellar mass). This letter will have a subscript in capital letters representing the quantity for which we give a prescription. As an example, to express a quantity A as a function of the stellar mass M_\star , we will write

$$A \propto M_\star^{m_A}. \quad (8)$$

2.4. Mass loss prescription

Because of the wind torque parametrization and the stellar magnetic field prescription, for the sake of consistency we will consider a power-law expression of the stellar mass loss

$$\dot{M} \propto \left(\frac{Ro}{Ro_\odot}\right)^{-p_M} \left(\frac{R_\star}{R_\odot}\right)^{r_M} \left(\frac{M_\star}{M_\odot}\right)^{m_M}, \quad (9)$$

where p_M, m_M & r_M will be constrained later. Note that those exponents follow the nomenclature presented in Section 2.3. However, the mass loss can be obtained from coronal quantities through a wind model, for example by assuming a radial polytropic pressure-driven outflow, with an index γ (cf. Appendix A):

$$\dot{M} \propto \left(\frac{M_\star}{M_\odot}\right)^2 \left(\frac{n_c}{n_\odot}\right) \left(\frac{T_c}{T_\odot}\right)^{-\frac{3}{2}} \left[1 - \frac{T_{\min,\odot}}{T_\odot} \frac{M_\star}{M_\odot} \frac{R_\odot}{R_\star} \frac{T_\odot}{T_c}\right]^{\frac{5-3\gamma}{2(\gamma-1)}}, \quad (10)$$

where n_\odot, T_\odot are respectively the solar values of the density and temperature at the base of the corona. $T_{\min,\odot} = (1 - 1/\gamma) Gm_p M_\odot / 2k_B R_\odot \approx 11 (1 - 1/\gamma)$ MK is the minimal temperature needed at the base of the corona for the Sun to obtain a transsonic wind. For instance, for $\gamma = 1.05$, value commonly used in the literature (Matt et al. 2012; Réville et al. 2015a; Finley & Matt 2017), we have $T_{\min,\odot} \approx 0.52$ MK. Such an expression will be used in Section 3.5.

2.5. General formulation of the torque

The parametrization of the torque with equation (6), together with the power-law expressions of the stellar magnetic field and the mass loss (equations (7) and (9)) lead to the following formulation of the torque as a function of fundamental stellar parameters

$$\Gamma_{\text{wind}} \propto Ro^{-4m.p_B - (1-2m)p_M} R_\star^{2+5m+4m.r_B + (1-2m)r_M} \times M_\star^{-m+4m.m_B + (1-2m)m_M} \frac{\Omega_\star}{\left(1 + \frac{f^2}{K^2}\right)^m}. \quad (11)$$

From this generic formulation, it is now possible to constrain the different exponents by taking into account several observational trends.

3. Observational constraints

3.1. Relationships between stellar parameters

Some observational trends are based on a set of main-sequence stars in the unsaturated rotation regime (for which the Rossby number is greater than a certain threshold) and therefore take into account scaling laws between stellar parameters, depending on a specific stellar evolution model. In particular we need to consider mass-radius and mass-luminosity relationships during the Main Sequence. We assume here the general correlations

$$L_\star \propto M_\star^\eta \quad (12)$$

$$R_\star \propto M_\star^\xi, \quad (13)$$

where η and ξ are constants which depend on which stellar model is considered. Therefore, the upcoming formulations, only valid during the Main Sequence, can accommodate any evolutionary model. We will by default use the typical values $\eta = 4$ and $\xi = 0.9$ (Kippenhahn & Weigert 1994).

3.2. Constraints from stellar rotational evolution

As already introduced, stellar spin-down studies in open clusters (first performed on the Pleiades, Ursa Major, and the Hyades) show that the rotation rate of evolved main sequence stars tends to converge to the solar rate on a sequence where $\Omega_\star \propto t^{-1/2}$ (Skumanich 1972). By assuming that the moment of inertia of the star is constant, the wind braking torque is constrained in the unsaturated regime to scale as the cube of the stellar rotation rate

$$\Gamma_{\text{wind}} \propto \Omega_\star^3. \quad (14)$$

In the following sections, we will assume that gyrochronology is valid thanks to the Skumanich law. This way, if a decrease of the wind braking efficiency is genuinely happening for evolved stars (van Saders et al. 2016), then we will only consider solar-type stars younger than the Sun to ensure the validity of equation (14). Note that a stalling of the magnetic braking could be modelled in our formalism with a *re-saturation* regime where the Rossby number is greater than a certain threshold Ro_{break} .

Matt et al. (2015) studied in more details the different dependencies of the wind braking torque to explain some characteristic features of the distribution of stellar rotation periods in open clusters and *Kepler* stars as a function of their mass. To this end, they focus on two kinds of stellar populations: the slow rotators, in an unsaturated regime, and the fast saturated rotators. The saturation threshold is given by a value of the Rossby number Ro_{sat} , which is assumed to be independent of any stellar parameters, at least at zeroth-order. To explain the mass dependency of the stellar spin-down, they take into account the Skumanich law in the unsaturated regime and a linear saturation for the wind braking torque, leading to the following prescription

$$\Gamma_{\text{wind}} = \Gamma_\odot \left(\frac{R_\star}{R_\odot}\right)^a \left(\frac{M_\star}{M_\odot}\right)^b \left(\frac{Ro}{Ro_\odot}\right)^{-2} \left(\frac{\Omega_\star}{\Omega_\odot}\right) \quad (\text{unsaturated}) \quad (15)$$

$$\Gamma_{\text{wind}} = \Gamma_{\odot} \left(\frac{R_{\star}}{R_{\odot}} \right)^a \left(\frac{M_{\star}}{M_{\odot}} \right)^b \left(\frac{Ro_{\text{sat}}}{Ro_{\odot}} \right)^{-2} \left(\frac{\Omega_{\star}}{\Omega_{\odot}} \right) \quad (\text{saturated}), \quad (16)$$

with $\Gamma_{\odot} = 6.3 \times 10^{30}$ erg, $a = 3.1$ and $b = 0.5$.

This prescription can be compared with our formulation, in equation (11), by assuming $f \ll 1$ and neglecting secular changes of the stellar parameters. It is thus possible to link the magnetic field of the star and the mass loss through the following conditions

$$p_B = \frac{1}{2m} - \frac{1-2m}{4m} p_{\dot{M}} \quad (\text{unsaturated}) \quad (17)$$

$$p_B = -\frac{1-2m}{4m} p_{\dot{M}} \quad (\text{saturated}) \quad (18)$$

$$r_B = \frac{a - (2+5m)}{4m} - \frac{1-2m}{4m} r_{\dot{M}} \quad (19)$$

$$m_B = \frac{b+m}{4m} - \frac{1-2m}{4m} m_{\dot{M}}. \quad (20)$$

Equation (17) is similar to the condition obtained by Skumanich (2019), if we take $p_B = 1/\beta$ & $p_{\dot{M}} = \alpha/\beta$, according to his notation. However, no correlation between B_{\star} and \dot{M} is assumed here. The wind torque parametrization therefore gives us the opportunity to infer the mass loss prescription from the magnetic field prescription and reciprocally.

In Figure 2 we illustrate the interdependencies in this first set of exponents. More precisely, the p_B exponent is expressed as a function of $p_{\dot{M}}$ from equation (17) for a dipolar field (solid black line), a quadrupolar field (dashed black line) and an octupolar field (dotted black line) in the case of an unsaturated rotation regime. The dashed blue lines correspond to magnetic field prescriptions from See et al. (2017) [S17] and Vidotto et al. (2014) [V14]. The blue crosses represent the magnetic field and mass loss prescriptions from Johnstone et al. (2015b) [J15], Tu et al. (2015) [T15], Sadeghi Ardestani et al. (2017) (*resp.* J15, T15, SA17). Those scaling laws have been derived to reproduce rotation rates of open clusters and are quite in agreement with a square root spin-down law. As already pointed out by Skumanich (2019), a wide range of exponents is admissible from the different prescriptions considered.

The magnetic topology has also a significant influence on the $\dot{M} - B_{\star}$ prescriptions. Indeed, the value of the m exponent decreases with an increasing complexity of the topology, corresponding to higher-order multipoles (Réville et al. 2015a). We will take here $m = 0.15$ for a quadrupolar field (see the dashed black line in Figure 2) and $m = 0.11$ for an octupolar field (see the dotted black line in Figure 2). More complex magnetic fields lead to steeper slopes in Figure 2 and therefore to a less constrained magnetic field. The mass loss, for its part, tends to be proportional to Ro^{-2} . Only one prescription of B_{\star} and \dot{M} is compatible with the Skumanich law for any magnetic topology (see the dark red dashed lines in Figure 2) and corresponds to the one highlighted by Skumanich (2019). This configuration leads to a linear magnetic field-rotation relation and a quadratic mass loss-rotation relation. This way, such a prescription may be used as a first estimate of B_{\star} and \dot{M} based on spin-down

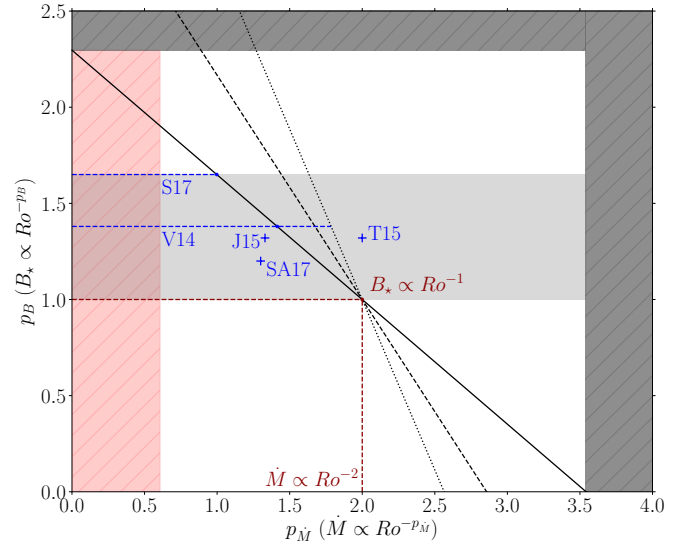


Fig. 2. Correlation $p_B - p_M$ for a dipolar (solid black line), a quadrupolar (dashed black line) and an octupolar (dotted black line) topology in the unsaturated regime. Dashed blue lines: magnetic field prescriptions from See et al. (2017) [S17] and Vidotto et al. (2014) [V14]. Blue crosses: magnetic field and mass loss prescriptions from Johnstone et al. (2015b) [J15], Tu et al. (2015) [T15] and Sadeghi Ardestani et al. (2017) [SA17]. In dark grey: excluded region in the dipolar case. Dashed dark red lines: prescriptions compatible with the Skumanich law for any magnetic topology. In light red: exponents corresponding to mass losses outside the envelope of Wood et al. (2005) data. The light grey band corresponds to the upper and lower bounds from ZDI statistical studies (see §3.4 for more details).

considerations without having to assume a particular magnetic topology. However, in the following sections, we will keep unspecified prescriptions for the magnetic field and the mass-loss rate in order to study the influence of additional observational constraints. It is important to note that complex fields can significantly modify the wind braking torque itself (Réville et al. 2015a; Garraffo et al. 2016). Furthermore, from those considerations, Garraffo et al. (2018) were able to reproduce the bimodal distribution of slow and fast rotators.

Since the dipole component tends to dominate the wind braking torque for mixed geometries (Finley & Matt 2018), such a topology is assumed by default in the following sections.

3.3. Constraints on the mass-loss rate

Given the one-to-one correspondence between the B_{\star} and \dot{M} exponents, constraints on the mass loss will affect the magnetic field and reciprocally. First, the mass loss is enhanced by stellar rotation (Wood et al. 2005; Suzuki et al. 2013; Holzwarth & Jardine 2007), leading to $p_{\dot{M}} \geq 0$. Therefore, we obtain

$$p_B \leq \frac{1}{2m} \approx 2.3 \quad (\text{unsaturated}) \quad (21)$$

$$p_B \leq 0 \quad (\text{saturated}). \quad (22)$$

Furthermore, Wood et al. (2002, 2005) showed a correlation between the mass loss and the X-ray stellar flux F_X for unsaturated main-sequence stars, expressed as

$$\dot{M} \propto R_{\star}^2 F_X^w, \quad (23)$$

where w is a constant between $w_{\min} \approx 0.3$ and $w_{\max} \approx 1.9$, to be consistent with Wood et al. (2005) observations. To convert this correlation into a $\dot{M}(Ro, R_*, M_*)$ prescription, we consider a relationship between the coronal activity and the stellar rotation, for unsaturated main-sequence stars:

$$\frac{L_X}{L_*} \propto Ro^{-p_L}, \quad (24)$$

with L_X the X-ray stellar luminosity, L_* the luminosity of the star and p_L an exponent between $p_{L,\min} = 2$ and $p_{L,\max} = 3$ (Pizzolato et al. 2003; Wright et al. 2011; Reiners et al. 2014). If we take into account the scaling laws from Section 3.1, it is possible to estimate the mass loss as a function of the Rossby number and the stellar mass from stellar activity considerations. Indeed, the X-ray flux becomes

$$F_X \propto Ro^{-p_L} M_*^{\eta-2\xi}, \quad (25)$$

which leads to the mass loss

$$\dot{M} \propto Ro^{-p_L w} M_*^{(\eta-2\xi)w+2\xi}. \quad (26)$$

By identification, the exponents of \dot{M} can be inferred from the set $\{\eta, \xi, p_L, w\}$:

$$p_{\dot{M}} = p_L w \quad (27)$$

$$\xi r_{\dot{M}} + m_{\dot{M}} = (\eta - 2\xi)w + 2\xi. \quad (28)$$

To be consistent with Wood et al. (2005) data, the most flexible constraint on the $p_{\dot{M}}$ exponent can be obtained from equation (27) as

$$0.6 \leq p_{\dot{M}} \leq 5.7. \quad (29)$$

According to equation (29), the values of $p_{\dot{M}}$ leading to (F_X, \dot{M}) outside the envelope of Wood et al. (2005) data define the exclusion red regions in Figure 2 and 3. Equations (27) and (28) then give an additional constraint on the different exponents of the mass loss prescription

$$\xi r_{\dot{M}} + m_{\dot{M}} - 2\xi = \frac{\eta - 2\xi}{p_L} p_{\dot{M}}. \quad (30)$$

This will dictate itself the mass and radius dependency of the stellar magnetic field, easier to observe, through equations (17) to (20), such that

$$4m(\xi r_B + m_B) = \xi(a - m - 4) + b + m - \frac{\eta - 2\xi}{p_L} (2 - 4mp_B). \quad (31)$$

Equation (31) shows that the mass-radius dependency of the magnetic field can be inferred from its Rossby number dependency, as shown in Figure 3, where the green area represents the exponents of the magnetic field prescription compatible with the different constraints we considered. The negative values of $\xi r_B + m_B$ show that the magnetic field should decrease with the stellar mass, which seems to be in agreement with dynamo models and observations (Johns-Krull & Valenti 2000; Brun et al. 2015).

One can also notice in Figure 3 that a stronger Rossby number dependency, for high values of p_B , will lead to a weaker but non negligible dependency on stellar mass through the $\dot{M} - F_X$ correlation. Furthermore, by considering the different exclusion regions (see the hatched areas in Figure 3), we can infer that a

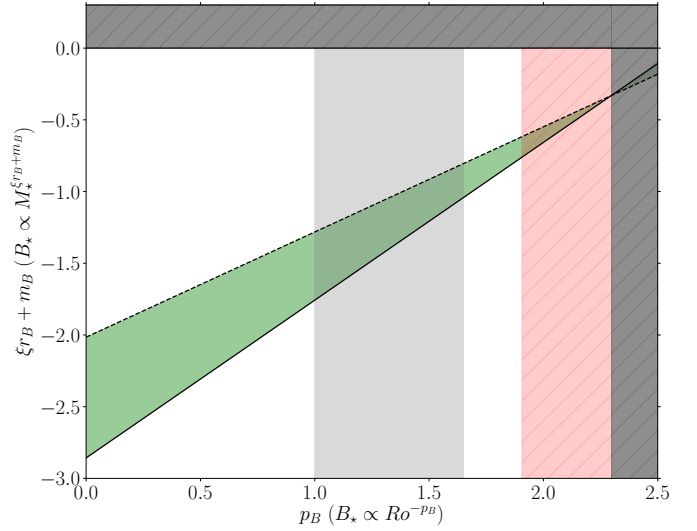


Fig. 3. Correlation between p_B and $\xi r_B + m_B$ in the unsaturated regime for $p_L = 2$ (black line) and $p_L = 3$ (dotted). Here, $\eta = 4$ and $\xi = 0.9$. In dark grey: excluded region. In red: exponents corresponding to mass losses outside the envelope of Wood et al. (2005) data. In green: exponents consistent with the mass-loss constraints. The light grey band corresponds to the upper and lower bounds from ZDI statistical studies (see §3.4 for more details).

magnetic field which is solely a function of the Rossby number (*i.e.* $r_B = m_B = 0$) cannot be consistent with the observed rotational dependency of L_X and \dot{M} , as well as with the $\dot{M} - F_X$ correlation. To fulfill this set of conditions, we need to add an explicit mass dependency to the stellar magnetic field.

Only a linear combination of r_B & m_B is here constrained, because of the mass-radius relationship. However, it is possible to discriminate the mass and radius dependencies by considering the magnetic topology.

3.4. Constraints on the magnetic field

The stellar magnetic field can be constrained in a variety of ways. Spectropolarimetric studies have exhibited correlations between the large scale magnetic field and other stellar parameters. For example, in Vidotto et al. (2014), B_* is shown to scale as $Ro^{-1.38 \pm 0.14}$, which leads to a mass loss $p_{\dot{M}} = -1.41 \pm 0.22$. The X-ray luminosity of the star can also be considered to infer the magnetic field. We assume here a correlation $L_X - B_*$ such that (Petsov et al. 2003; Vidotto et al. 2014)

$$\frac{L_X}{L_*} \propto B_*^v, \quad (32)$$

which leads to $p_B = p_L/v$. Assuming for instance $p_B = -1.38 \pm 0.14$ and $p_L = 2.5 \pm 0.5$ leads to $v = 1.81 \pm 0.6$, to be compared with the value $v = 1.61 \pm 0.15$ obtained in Vidotto et al. (2014) through a power-law fit.

Since the magnetic field is enhanced by the stellar rotation (Noyes et al. 1984; Brandenburg & Saar 2000; Petit et al. 2008), the exponent p_B has to be nonnegative, leading to the following constraint on the mass-loss rate in the unsaturated regime

$$p_{\dot{M}} \leq \frac{2}{1 - 2m} \approx 3.5. \quad (\text{unsaturated}) \quad (33)$$

At saturation, with equation (22), such a condition gives $p_B = 0$ & $p_{\dot{M}} = 0$, which means a mass loss and a magnetic field independent of the stellar rotation rate.

We will consider in the following sections lower and upper bounds for the values of p_B and p_M , in order to be consistent with observational trends. Measured stellar magnetic field, from Zeeman broadening and ZDI studies (Montesinos & Jordan 1993; Vidotto et al. 2014; See et al. 2017), only exhibited linear or super-linear dependencies between the large-scale magnetic field and the Rossby number. We will then take $p_B \geq 1$ to take this fact into account. The See et al. (2017) prescription, *i.e.* $p_B = 1.65$, will be used as an upper bound. The values of all the exponents associated to these two scenarii are given in Table 1. It is a common knowledge that ZDI maps, representing the large-scale unsigned magnetic flux, do not give any information about the small-scale magnetic field, that might be dominant for young fast rotating stars. However, a correlation between measurements from Zeeman-Doppler Imaging and Zeeman Broadening (See et al. 2019) gives some confidence in the general trends found in the literature.

The bounds we assumed above are greater than the exponents predicted by some scaling laws for stellar dynamos ($p_B = 0$ for the equipartition, $p_B = 1/4$ for the buoyancy regime and $p_B = 1/2$ for the magnetostrophy regime ; for a review, see Augustson et al. 2017a). This discrepancy likely comes from the fact that dynamo scaling laws and ZDI observations do not relate to the same magnetic field. The measured magnetic field from ZDI studies corresponds to the average unsigned photospheric flux $\langle B_V \rangle$, which is an estimate of the large scale magnetic field at the stellar surface. Dynamo-based scaling laws aim to estimate the stellar magnetic field over a wide spectral range. The latter can be linked to the average unsigned surface field strength, $\langle B_I \rangle$, obtained from Zeeman broadening, by means of a filling factor f representing the fraction of the stellar surface which is magnetized (see Reiners (2012) for more details). See et al. (2019), by exhibiting a correlation between $\langle B_V \rangle$ and $\langle B_I \rangle$, estimated a filling factor from a dynamo-produced magnetic field in the equipartition regime and showed a strong Rossby number dependency of their f estimate, which could be an avenue towards the explanation of this difference.

In a nutshell, it is possible by relying on a wind torque parametrization to provide B_\star and \dot{M} estimates consistent with spin-down and X-ray emission constraints (cf. equations (17) to (20) and equation (31)), given for example the $B_\star - Ro$ relation (*i.e.* the p_B exponent). In a quest to better understand the link between stellar and wind properties, we will expand our set of prescriptions to probe the coronal properties of the star by relying upon a wind model.

3.5. Constraints on the coronal properties

3.5.1. Probing the coronal properties: the role of magnetic topology

As seen in the previous section, the mass loss behavior can be constrained by the stellar magnetic field and the wind braking torque. This way, the knowledge of the \dot{M} expression will allow us to go further by inferring prescriptions for the coronal temperature and density, by means of the X-ray stellar emission. Indeed, their rotational dependency have often been constrained in the literature through the high-energy activity of the star (Mestel & Spruit 1987; Ivanova & Taam 2003; Holzwarth & Jardine 2007).

However, X-ray emission and wind acceleration (at least for the fast wind) are believed to arise from different regions in the corona (from dead zones and coronal holes respectively). Therefore, we will here assume that the coronal temperature T_c and

the base density n_c in the open-field regions are the quantities ruling the mass loss for a given wind model (cf. equation (10) for example), whereas the X-ray luminosity can be inferred from radiative losses by knowing the temperature T_l and the density n_l in closed-field regions (cf. Appendix B). In other words, the \dot{M} prescription from the previous sections allow us to link T_c and n_c , while the Rossby dependency of L_X , which has to be consistent with equation (24), correlates T_l and n_l . All those connexions are summarized in Figure 4. Since T_l can be obtained from observations (Preibisch 1997; Johnstone & Güdel 2015; Wood et al. 2018), we need an additional constraint to relate (T_c , n_c) to (T_l , n_l).

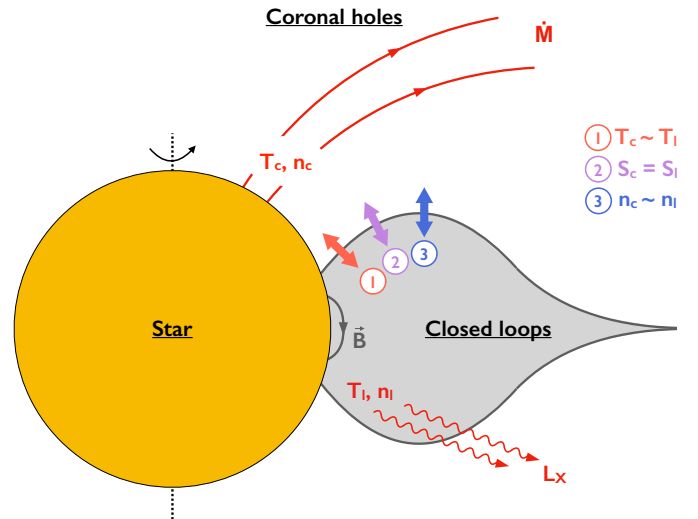


Fig. 4. Sketch of the coupling between the coronal temperature and density in the open-field and the closed-field regions, the X-ray luminosity and the mass-loss rate. Several scenarii are considered to connect the closed loops to the coronal holes. Scenario 1, in red: single temperature scaling. Scenario 2, in purple: entropy equilibrium. Scenario 3, in blue: single density scaling.

To this end, we will consider three scenarii to couple the open-field and the closed-field regions:

- *Scenario 1* (in red in Figure 4): we consider a common scaling law for T_c and T_l (Johnstone et al. 2015a; Ó Fionnagáin & Vidotto 2018) which leads to different scalings for the densities.
- *Scenario 2* (in purple in Figure 4): we assume an entropy equilibrium between the closed loops and the coronal holes.
- *Scenario 3* (in blue in Figure 4): we assume a common scaling for n_c and n_l (Ivanova & Taam 2003; Holzwarth & Jardine 2007; See et al. 2014) which leads to different scalings for the temperatures.

It is worth noticing that scenarii 1 and 3 lead to drastically different trends for the temperature T_c . Therefore, a scenario where both the density and the temperature possess the same scaling in the open and closed field regions is unrealistic.

Such an approach allows us to deal with the local magnetic field distribution in an admittedly simplified way, by distinguishing quiet open-field regions from closed loops associated to active regions. This distinction translates into different coronal temperature and density prescriptions, which are always

chosen to be compatible with our derived wind mass-loss rate in the polytropic formalism. Of course at the surface of the star the plasma dynamics and heating mechanisms are much more involved than in our simplified approach (Wedemeyer-Böhm et al. 2009). Still this is a first step to characterize the general properties of the coronae of cool stars, and we intend in the future to consider more realistic modeling for the detailed coronal heating mechanism.

In what follows, we will see how to constrain the coronal temperatures and densities from L_X and \dot{M} (Sections 3.5.2 and 3.5.3 respectively). Then, we will inventory the different scenarii in Sections 3.5.4, 3.5.5 and 3.5.6.

3.5.2. Coronal temperature and density: X-ray luminosity consistency

The temperature and the density in closed loops are connected to the X-ray luminosity, which has to be consistent with the prescriptions we already adopted (cf. equation (24)). From radiative losses considerations, the X-ray luminosity can be expressed as (cf. Appendix B)

$$L_X \propto \left(\frac{R_\star}{R_\odot}\right)^3 \left(\frac{B_\star}{B_\odot}\right) \left(\frac{n_l}{n_{l,\odot}}\right)^{\frac{3}{2}} \left(\frac{T_l}{T_{l,\odot}}\right)^{-\frac{7}{6}}. \quad (34)$$

In order to standardize the different prescriptions, we will consider a power-law expression for the temperature and the density in the dead zones, *i.e.*

$$T_l \propto \left(\frac{Ro}{Ro_\odot}\right)^{-p_{T,l}} \left(\frac{R_\star}{R_\odot}\right)^{r_{T,l}} \left(\frac{M_\star}{M_\odot}\right)^{m_{T,l}}, \quad (35)$$

$$n_l \propto \left(\frac{Ro}{Ro_\odot}\right)^{-p_{n,l}} \left(\frac{R_\star}{R_\odot}\right)^{r_{n,l}} \left(\frac{M_\star}{M_\odot}\right)^{m_{n,l}}. \quad (36)$$

Furthermore, for main-sequence stars in the unsaturated regime, we will assume a correlation between the X-ray flux and the coronal temperature in the closed loops such that (Preibisch 1997; Johnstone & Güdel 2015; Wood et al. 2018)

$$T_l \propto F_X^{j_l}, \quad (37)$$

with an exponent $j_l = 0.26$ (Johnstone & Güdel 2015). Equation (25), with relationships from Section 3.1, then result in a $T_l(Ro, M_\star)$ formulation

$$T_l \propto Ro^{-p_L j_l} M_\star^{(\eta-2\xi)j_l}. \quad (38)$$

This leads by identification to

$$p_{T,l} = p_L j_l. \quad (39)$$

The rotational dependency of the density can therefore be deduced from the magnetic field prescription for a given set $\{p_L, j_l\}$ by ensuring the consistency with equation (24):

$$p_{n,l} = \frac{2}{3}(p_L - p_B) + \frac{7}{9}p_L j_l. \quad (40)$$

The X-ray luminosity therefore gives us the possibility to constrain the Rossby dependency of the temperature and the density in closed loops.

We now need to study the connection between the X-ray luminosity and the temperature in coronal holes, which will allow us to infer the mass-radius dependency of T_c from its rotational

dependency, as we did for the mass-loss rate in Section 3.3. X-ray emission and wind acceleration have similar sources closely linked to the heating of the corona, which is probably due to the transport of energy from the photosphere through weakly dissipative Alfvén waves. These phenomena involve steep density gradients (Heyvaerts & Priest 1983) and nonlinear interactions between inward and outward perturbations (Velli et al. 1989), among others (for a review, see Mathioudakis et al. 2013; Cranmer, Gibson & Riley 2017). While this process is efficient in closed loops thanks to the magnetic topology, it requires wave reflections *e.g.* through the parametric instabilities in coronal holes (Réville et al. 2018), reducing the heating efficiency in those regions. To take this behavior into account, we will assume a correlation between the X-ray flux and the coronal temperature T_c like in the closed loops case, with an unspecified exponent, different from j_l because of the possible difference of heating efficiency between open-field and closed-field regions.

3.5.3. Coronal temperature and density: polytropic wind model considerations

The temperature and the density in coronal holes need to be consistent with our mass loss prescription, constrained in Sections 3.1 to 3.4. We will consider the following power-law expression for the coronal temperature:

$$T_c \propto \left(\frac{Ro}{Ro_\odot}\right)^{-p_T} \left(\frac{R_\star}{R_\odot}\right)^{r_T} \left(\frac{M_\star}{M_\odot}\right)^{m_T}. \quad (41)$$

Such a prescription has to fulfill the condition $\dot{M} > 0$, which defines a maximal value for the p_T exponent (see Appendix C for more details).

Knowing the value of T_c for a given wind model, it is possible to infer the coronal density to obtain a consistent mass-loss rate. As we saw in Section 2.4 with the equation (10), the mass loss can be expressed as a function of stellar parameters and coronal properties. To be consistent with the power-law prescription from equation (9), the coronal density n_c has to be expressed as

$$n_c \propto Ro^{-p_M} R_\star^{r_M} M_\star^{m_M-2} T_c^{\frac{3}{2}} \left[1 - \frac{T_{\min,\odot} M_\star R_\odot T_\odot}{T_\odot M_\odot R_\star T_c}\right]^{\frac{3\gamma-5}{2(\gamma-1)}}. \quad (42)$$

It is important to keep in mind that this equation is valid if $c_s/v_{\text{esc}} \ll 1$, where c_s is the speed of sound in the stellar corona, and v_{esc} the escape velocity at the stellar surface (cf. Appendix A). In the light of this condition, high coronal temperatures could invalidate this analytical expression of n_c .

If we assume that the coronal temperature varies slightly for the stellar parameters we consider, we can approximate this expression to a power law on the Main Sequence such that (see details in Appendix D)

$$n_c \propto \left(\frac{Ro}{Ro_\odot}\right)^{-p_n} \left(\frac{R_\star}{R_\odot}\right)^{r_n} \left(\frac{M_\star}{M_\odot}\right)^{m_n}, \quad (43)$$

with:

$$p_n = p_M + \left(\frac{3}{2} - F(\gamma)\right) p_T, \quad (44)$$

$$r_n = r_M + \frac{3}{2} r_T - F(\gamma)(1 + r_T), \quad (45)$$

$$m_n = m_{\dot{M}} - 2 + \frac{3}{2}m_T - F(\gamma)(m_T - 1) \quad (46)$$

$$\text{and } F(\gamma) = \frac{5 - 3\gamma}{2(\gamma - 1)} \frac{T_{\min,\odot}/T_\odot}{1 - T_{\min,\odot}/T_\odot}. \quad (47)$$

Therefore, for a given mass-loss rate prescription, a one-to-one correspondence between $\{p_T, r_T, m_T\}$ and $\{p_n, r_n, m_n\}$ occurs by considering a pressure-driven polytropic wind. Furthermore, we are able to infer $\xi r_T + m_T$ from the p_T exponent thanks to a $T_c - F_X$ correlation (cf. Appendix C). Given that the Rossby dependency of T_l and n_l is already known through equations (39) and (40) respectively, we only need one additional constrain to fully determine the expression of T_c and n_c . We choose here to connect the rotational dependency of the temperature and the density in open and closed regions by means of the three scenarii we presented in Section 3.5.1. We detail now the implications of these scenarii in sections 3.5.4, 3.5.5 and 3.5.6.

3.5.4. Scenario 1: single temperature scaling

To connect closed loops to coronal holes, we can adopt a single scaling law for the temperature (*i.e.* $T_l \propto T_c$), leading to a same X-ray flux-temperature correlation in both regions. This way, the Johnstone & Güdel (2015) prescription, coupled with the $L_X - Ro$ relation and the results from Section 3.1, provides a complete expression for T_c . One can not assume weak variations of the coronal temperature, which means that a power-law expression for n_c may be a loose approximation in this scenario (cf. Appendix D). However, the coronal density can be inferred directly from our wind model through equation (42), in order to keep a consistent mass loss. Those considerations then allow us to estimate T_c and n_c by means of the following prescriptions

$$p_T = p_L j_l, \quad (48)$$

$$\xi r_T + m_T = \frac{\eta - 2\xi}{p_L} p_T, \quad (49)$$

$$n_c \propto Ro^{-p_M} R_\star^{r_M} M_\star^{m_M - 2} T_c^{\frac{3}{2}} \left[1 - \frac{T_{\min,\odot}}{T_c} \frac{M_\star}{M_\odot} \frac{R_\odot}{R_\star} \right]^{\frac{3\gamma - 5}{2(\gamma - 1)}}. \quad (50)$$

In a saturated rotation regime, it is impossible from equation (50) to keep a constant value for both T_c and n_c . We will assume by simplicity a single temperature at saturation, the corresponding coronal density being inferred from the \dot{M} prescription.

The robustness of the single temperature scaling hypothesis can nevertheless be questioned. In closed loops, available estimates of T_l (Preibisch 1997; Johnstone & Güdel 2015; Wood et al. 2018) fall back on an emission measure weighted average coronal temperature, based on heavy ions emission (Güdel 2007). From the wind model point of view, based on the modelling of a perfectly ionized hydrogen gas, the electron temperature (which is in this context similar to the proton temperature) is required to compute the mass-loss rate. Thus, a single scaling law for both temperatures may appear as a loose assumption. Indeed, if different radial profiles of temperature are observed in the solar wind for these two populations (Cranmer, Gibson

& Riley 2017), with a higher temperature for heavy ions, their dependency on stellar parameters is still unknown.

Furthermore, if we assume $T_c \propto T_l$, slower rotators may have a colder corona, leading to extremely strong densities to keep a consistent mass loss. As an example, for a solar twin with a rotation period of 56 days, the single temperature scaling scenario leads to $n_c \approx 19.58 n_\odot$, which has to be compared to $n_l \approx 0.48 n_\odot$, according to equation (40). Coronal holes of slow rotators would be abnormally dense, which may suggest that a single scaling law for the temperature might be inconsistent with the other hypothesis of our formalism, especially the choice of our wind model. Because of those points we will consider other scenarii in what follows.

3.5.5. Scenario 2: entropy equilibrium

A second possibility is to assume entropy equilibrium between closed and open field regions allowing both density and temperature to vary simultaneously. This allows us to derive the following relation:

$$\ln T_l - (\gamma_{ad} - 1) \ln n_l = \ln T_c - (\gamma_{ad} - 1) \ln n_c, \quad (51)$$

where $\gamma_{ad} = c_p/c_v = 5/3$ is the standard adiabatic exponent for an ideal gas. If we assume a power-law expression for n_c as in equation (43), this balance then gives for the Rossby dependency of the temperatures and densities:

$$p_{T,l} - (\gamma_{ad} - 1)p_{n,l} = p_T - (\gamma_{ad} - 1)p_n. \quad (52)$$

Along with equation (44) ruling the rotational dependency of the mass-loss rate in our wind model, one can express the p_T and p_n exponents as follows:

$$p_T = \frac{(\gamma_{ad} - 1)(p_{n,l} - p_M) - p_L j_l}{(\gamma_{ad} - 1)[3/2 - F(\gamma)] - 1}, \quad (53)$$

$$p_n = p_M + \left(\frac{3}{2} - F(\gamma) \right) p_T. \quad (54)$$

The $T_c - F_X$ correlation (cf. Appendix C), along with the wind model through equations (45) and (46), dictate the mass-radius dependency of T_c and n_c as

$$\xi r_T + m_T = \frac{\eta - 2\xi}{p_L} p_T \quad (55)$$

$$\xi r_n + m_n = \xi r_M + m_M - 2 + (\xi r_T + m_T) \left[\frac{3}{2} - F(\gamma) \right] + (1 - \xi) F(\gamma) \quad (56)$$

Equations (53) to (56) then define the power-law expressions of T_c and n_c for this scenario.

At high rotation rates, we have seen in Section 3.3 that the linear saturation of the wind braking torque leads to a magnetic field and a mass loss independent of the Rossby number, *i.e.* $p_B = p_{\dot{M}} = 0$. A similar behavior has been observed for the X-ray activity of stars (Pizzolato et al. 2003; Wright et al. 2011). We assume here for simplicity that $p_L = 0$ in the saturated regime. We can show by relying on calculations similar to those presented in Sections 3.5.2 and 3.5.3 that $p_n = p_T = 0$ is an acceptable choice if we assume a similar behavior in closed loops.

3.5.6. Scenario 3: single density scaling

Let us finally consider that the coronal density has a similar behavior in the closed-field and open-field regions. This way, two different scaling laws will arise for the temperatures in closed or open-field regions. In this case, the coronal density n_c , launching the wind in the open-field regions, is proportional to the density in closed loops n_l , and therefore can be expressed as a power law with a Rossby exponent given by equation (40) to ensure a consistent X-ray luminosity. Considering a power-law expression for n_c is a reasonable assumption if the temperature in coronal holes presents only small variations with respect to stellar parameters (cf. Appendix D). Such a supposition seems to be consistent with Suzuki et al. (2013), who performed simulations of flux tubes heated by Alfvén wave dissipation in coronal holes. Indeed, they predicted a weak dependency of the coronal temperature on the stellar magnetic field, which can be extrapolated to more fundamental stellar parameters through a dynamo relationship (see equation (7)). We can now infer the expression of the Rossby-dependency of the coronal temperature (*i.e.* the p_T exponent) through equation (44). All those aspects allow us to determine the rotational dependency of T_c and n_c thanks to the following prescriptions

$$p_n = \frac{2}{3}(p_L - p_B) + \frac{7}{9}p_L j_l, \quad (57)$$

$$p_T = \frac{p_n - p_M}{\frac{3}{2} - F(\gamma)}. \quad (58)$$

As for the entropy equilibrium scenario, the mass-radius dependency of T_c and n_c is determined through the wind model and the $T_c - F_X$ correlation (cf. Appendix C):

$$\xi r_T + m_T = \frac{\eta - 2\xi}{p_L} p_T, \quad (59)$$

$$\xi r_n + m_n = \xi r_M + m_M - 2 + (\xi r_T + m_T) \left[\frac{3}{2} - F(\gamma) \right] + (1 - \xi) F(\gamma). \quad (60)$$

Equations (57) to (60) therefore give us the possibility to estimate the coronal temperature and density in open regions.

Like in Section 3.5.5, the assumption of a coronal temperature and density independent of the Rossby number in the saturated rotation regime is consistent with the different observational constraints we imposed.

Figure 5 shows the T_c and n_c estimates for a solar twin with a rotation period of 15 days (corresponding to $Ro = 0.6$ in the Sadeghi Ardestani et al. (2017) prescription) in the three physical scenarii we analyzed. We set $\eta = 4$, $\xi = 0.9$ (Kippenhahn & Weigert 1994), $\gamma = 1.05$ and $T_\odot = 1.5$ MK (Réville et al. 2016). One can notice that a stronger dependency of the magnetic field on the Rossby number, *i.e.* higher values of p_B , leads to weaker values of T_c and n_c (apart from the coronal temperature in Scenario 1 which remains constant; see the light red band in panel A of Figure 5). Furthermore, coronal temperatures obtained in scenarii 2 and 3 (see the blue and purple bands in panel A of Figure 5) only vary a little around the solar value, which is consistent with the assumptions we made to express n_c as a power law. Since the star we consider here is a solar twin rotating more rapidly (*i.e.* with $Ro/Ro_\odot < 1$), the positiveness criterion of the

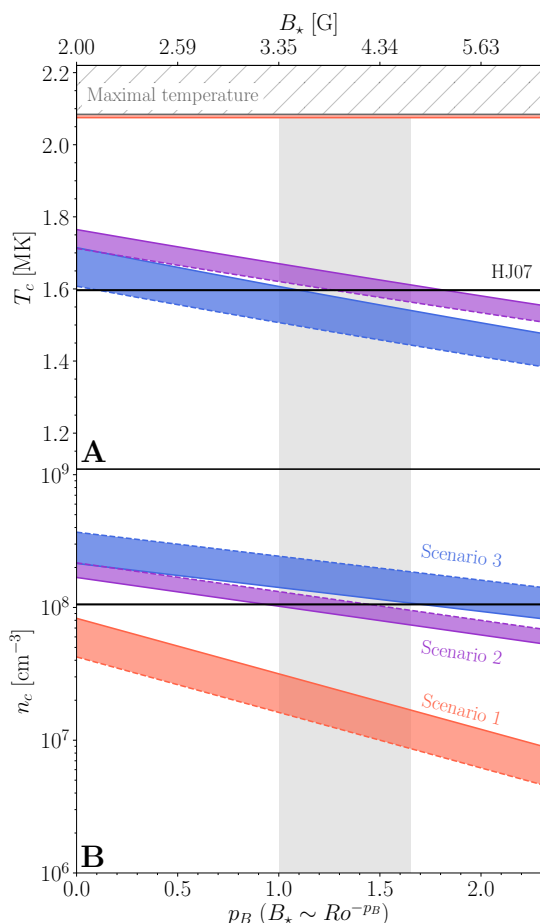


Fig. 5. Evolution of T_c (panel A) and n_c (panel B) as a function of p_B , for a solar twin with a rotation period of 15 days. Solid line: $p_L = 2$. Dashed lines: $p_L = 3$. In black: Holzwarth & Jardine (2007) prescription. In light red: single temperature scaling scenario. In purple: entropy equilibrium scenario. In blue: single density scaling scenario. In hatched grey: values of coronal temperatures leading to $\dot{M} < 0$. The light grey band corresponds to the upper and lower bounds of p_B we consider to be consistent with ZDI statistical studies.

mass-loss rate (cf. Appendix C) sets a maximal coronal temperature (see the dark grey line in panel A of Figure 5). From this condition, one can affirm that scenarii 2 and 3 are compatible with a transsonic wind. However, in scenario 1, the condition $\dot{M} > 0$ is only ensured for $p_L \approx 2$, the coronal temperature being too high otherwise given a reasonable choice of (γ, T_\odot) .

Considering our lower and upper bounds for p_B as described in Section 3.4, single density scaling and entropy equilibrium lead to coronal temperatures close to the Holzwarth & Jardine (2007) prescription (see the black horizontal line in Figure 5). Scenario 3 leads to temperatures weaker than the predicted value of Holzwarth & Jardine (2007), resulting in slightly higher densities for a given mass-loss rate (see the blue band in panel B of Figure 5). On the contrary, marginally higher temperatures and lower densities can be observed in scenario 2 (see the purple band in panel B of Figure 5). Scenario 3, with a T_c prescription independent of the magnetic field and the mass-loss scaling laws, leads up to the highest values of the coronal temperature and the lowest values of the coronal density shown in Figure 5 (in light red in Figure 5).

In the light of those different aspects, scenarii 2 and 3 seem more likely to account for a consistent stellar spin-down with a polytropic pressure-driven wind.

4. Scaling laws and observations of individual systems

4.1. Using our scaling laws: a practical guide

4.1.1. Rossby number and rotation regime

To deal with individual systems, we need to know their Rossby number to rely on our prescriptions. We will here use for the sake of simplicity the stellar Rossby number (cf. equation (1)) and more precisely the Sadeghi Ardestani et al. (2017) prescription for the convective turnover time. Following their approach, this characteristic time is defined as the ratio between the pressure scale height and the convective velocity estimated with the mixing length theory. They computed the relevant quantities at half a pressure scale height over the base of the convective zone and followed their evolution by means of the CESAM stellar evolution code (Morel & Lebreton 2008). The formulation they obtained has the advantage of being valid during the Pre-Main Sequence and the Main Sequence for metallicities ranging from $[\text{Fe}/\text{H}] = -0.5$ to 0.5 , by falling back on the stellar convective mass as the control parameter. Given the age of the system we will consider, such an expression can be simplified for main-sequence stars to depend only on the stellar mass and the stellar radius, which leads to the following formulation for the convective turnover time:

$$\tau_c \propto M_\star^{-1} R_\star^{-1.2}. \quad (61)$$

This prescription leads to a solar value $Ro_\odot = 1.113$ and a saturation value $Ro_{\text{sat}} = 0.09$.

4.1.2. Scaling laws: numerical values of the exponents

In the previous sections, we have been able to constrain the magnetic field, the mass loss, the coronal temperature and the coronal density from wind braking considerations, by assuming the following prescriptions (at least in the entropy equilibrium and the single density scaling scenarii):

$$\Gamma_{\text{wind}} \propto \dot{M}^{1-2m} B_\star^{4m} R_\star^{2+5m} M_\star^{-m} \Omega_\star \left[1 + \frac{f^2}{K^2} \right]^{-m} \quad (62)$$

$$B_\star \propto Ro^{-p_B} \left(\frac{R_\star}{R_\odot} \right)^{r_B} \left(\frac{M_\star}{M_\odot} \right)^{m_B} \quad (63)$$

$$\dot{M} \propto Ro^{-p_M} \left(\frac{R_\star}{R_\odot} \right)^{r_M} \left(\frac{M_\star}{M_\odot} \right)^{m_M} \quad (64)$$

$$T_c \propto Ro^{-p_T} \left(\frac{R_\star}{R_\odot} \right)^{r_T} \left(\frac{M_\star}{M_\odot} \right)^{m_T} \quad (65)$$

$$n_c \propto Ro^{-p_n} \left(\frac{R_\star}{R_\odot} \right)^{r_n} \left(\frac{M_\star}{M_\odot} \right)^{m_n} \quad (66)$$

As an example, the values of all the exponents linked to the lower and upper bounds we considered in Section 3.4 (namely $1 \leq p_B \leq 1.65$) are given in Table 1 for the single density scaling scenario (in blue in Figure 4). The corresponding exponents for the two other cases can be found in Appendix E. One can notice that the configuration for which $p_B = 1.65$ ("upper bound") leads to a mass-loss rate behavior similar to Holzwarth & Jardine

Table 1. Parameters defining the Γ_{wind} , B_\star , \dot{M} , T_c & n_c prescriptions for $p_B = 1$ and $p_B = 1.65$ in the single density scaling scenario.

Lower bound	Upper bound	Equation
<i>Free parameters.</i>		
$\gamma = 1.05^a$	-	(10)
$m = 0.2177^b$	-	(6)
<i>Constrained parameters.</i>		
$T_\odot = 1.5 \text{ MK}^a$	-	(10)
$\eta = 4^c$, $\xi = 0.9^c$	-	(12), (13)
$p_L = 2^d$	-	(24)
$a = 3.1^e$, $b = 0.5^e$	-	(15)
$p_B = 1$	$p_B = 1.65^f$	(7)
$\xi r_B + m_B = -1.76$	$\xi r_B + m_B = -1.04$	(7)
$p_M = 2$	$p_M = 1$	(9)
$\xi r_M + m_M = 4$	$\xi r_M + m_M = 2.9$	(9)
$w = 1$	$w = 0.5$	(23)
$p_T = 0.11$	$p_T = 0.04$	(58)
$\xi r_T + m_T = 0.12$	$\xi r_T + m_T = 0.05$	(59)
$j = 0.055$	$j = 0.02$	(C.1)
$p_n = 1.07$	$p_n = 0.64$	(57)
$\xi r_n + m_n = 1.97$	$\xi r_n + m_n = 1.49$	(60)

^(a) Réville et al. (2015b) ^(b) Matt et al. (2012) ^(c) Kippenhahn & Weigert (1994) ^(d) Pizzolato et al. (2003) ^(e) Matt et al. (2015) ^(f) See et al. (2017)

(2007), with $\dot{M} \propto R_\star^2 F_X^{0.5}$ and $\dot{M} \propto Ro^{-1}$ ($p_M = 1$). However, the difference observed in Section 3.5 regarding the rotational dependency of T_c and n_c arises partially from a reasonable choice of (γ, T_\odot) . Indeed, by considering as in their study $\gamma = 1.22$ and $T_\odot = 2.93 \text{ MK}$, we obtain $p_T = 0.074$ and $p_n = 0.64$, which is close to their published values $p_T = 0.1$ and $p_n = 0.6$.

Statistical ZDI studies, through the bounds of the p_B exponents, and prescriptions from spin-down considerations allow us to predict the admissible trends for the $\dot{M} - F_X$ correlation (cf. equation (23)). This is shown in Figure 6 as a light grey area along with the observed $\dot{M} \propto R_\star^2 F_X^w$ relationship initially published by Wood et al. (2005). One can notice that the predicted values of the w exponent are compatible with Wood et al. (2005) and Jardine & Collier Cameron (2019) observations. Furthermore, they present a bias towards active stars with low mass-loss rates leading to weaker slopes than the Wood et al. (2005) prescription of $w = 1.34$ (see the grey dotted line in Figure 6). Nevertheless, this behavior is in agreement with Suzuki et al. (2013) results which predicted an exponent $w = 0.82$ (see the red dashed line in Figure 6).

4.1.3. Normalization factors

If the exponents are fixed thanks to the previous calculations, the normalization of the scaling laws is still an open issue. By default, in the above analytical development, all the relevant quantities have been normalized to the solar values. However, we need to take into account additional constraints on each physical parameter in a solar configuration:

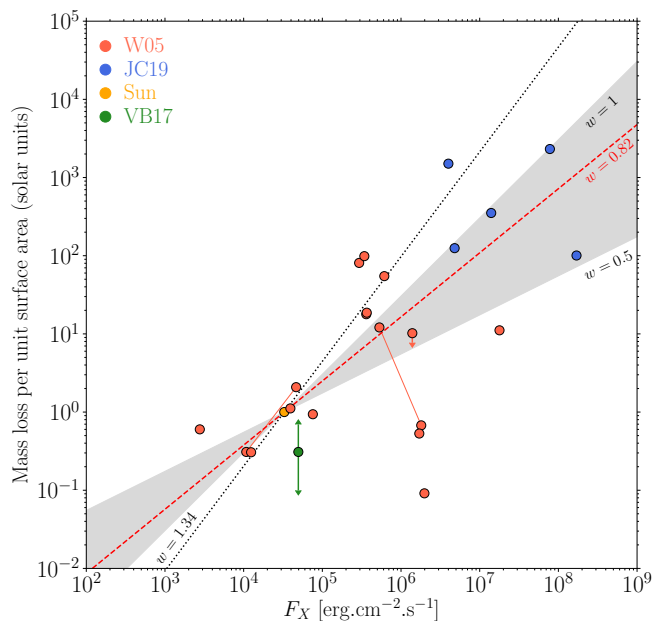


Fig. 6. Mass loss per unit area as a function of the X-ray flux. The red dots come from Wood et al. (2005) [W05] and the blue dots from Jardine & Collier Cameron (2019) [JC19]. In green: measurements from the atmospheric evaporation of GJ 436b (Vidotto & Bourrier 2017, VB17). Grey dotted line: Wood et al. (2005) scaling law corresponding to $w = 1.34$. Red dashed line: Suzuki et al. (2013) scaling law corresponding to $w = 0.82$. The light grey region corresponds to the upper and lower bounds we considered to be consistent with ZDI statistical studies.

- *Magnetic field.* ZDI studies show a significant scatter in the dataset used to exhibit correlations between the large scale magnetic field and other stellar parameters. Such a dispersion is here taken into account in the magnetic field normalization by considering the See et al. (2017) dataset, for which the average dipolar field strength at their value of the solar Rossby number lies between $B_{\odot} = 0.6$ and 4 G.
- *Mass-loss rate.* The value of \dot{M}_{\odot} is deduced from B_{\odot} by keeping a fixed solar wind torque, since $\Gamma_{\text{wind},\odot} \propto B_{\odot}^{4m} \dot{M}_{\odot}^{1-2m}$ (cf. equation (11)). This way, for $m = 0.22$, we have $7.9 \times 10^{-15} \leq \dot{M}_{\odot} [\text{M}_{\odot}.\text{yr}^{-1}] \leq 1.47 \times 10^{-13}$.
- *Coronal temperature.* The normalization of the coronal temperature and density is determined by performing 1D simulations of a pressure-driven polytropic wind with $\gamma = 1.05$, using the starAML routine (Réville et al. 2015b). The value of T_{\odot} is tuned to provide an average solar wind velocity at 1 AU of 444 km.s⁻¹, leading to $T_{\odot} = 1.5$ MK (Réville et al. 2016).
- *Coronal density.* The density at the base of the solar corona is then computed to be consistent with T_{\odot} and \dot{M}_{\odot} , which results in $2.49 \times 10^7 \leq n_{\odot} [\text{cm}^{-3}] \leq 4.63 \times 10^8$.

Once the exponents of the scaling laws and their normalization factors are well-defined, we now can compare the different prescriptions to observations of individual systems. We will focus on ZDI studies constraining the stellar magnetic field and mass loss measurements from astrospheres’ Ly α absorption.

4.2. A star studied through astrosphere’s Ly α absorption and Zeeman-Doppler Imaging: ϵ Eridani

We apply our formalism to ϵ Eridani, a young active K2V dwarf which hosts an exoplanet and a debris disk. We will study this individual system by only taking the minimal information required in our formalism, in order to test the different scaling laws. In practical terms, we only rely on the stellar mass and the rotation period, which are essential to use the different prescriptions (see Table 2 for numerical values of those stellar parameters). An estimate of the age indicates that the star is in the Main Sequence.

Table 2. Stellar parameters of ϵ Eridani.

Star	ϵ Eridani	
	Model Inputs	
$M_{\star} (M_{\odot})$	$0.856^{+0.006}_-0.008$ ^a	
$P_{\text{rot}} (d)$	11.68 ^a	
Age (Gyr)	0.44 ^a	
	Observations	Model Outputs
$R_{\star} (R_{\odot})$	0.74 ± 0.01 ^a	0.87 ^b
$L_{\star} (L_{\odot})$	0.34 ^c	0.54 ^b
$\log L_X (\text{erg}.\text{s}^{-1})$	28.32 ^d	28.24 ^b
Ro	-	0.28 ^b
$B_{\star} (G)$	6.15–19.8 ^{a,e}	3–47 ^b
$\dot{M} (10^{-14} M_{\odot}.\text{yr}^{-1})$	30–120 ^d	1.9–120 ^b

(^a) Jeffers et al. (2014) (^b) This work (Model) (^c) Saumon et al. (1996) (^d) Wood et al. (2002) (^e) See et al. (2017)

The stellar luminosity, the stellar radius and the X-ray luminosity can be estimated through equations (12), (13) and (24) (see Table 1 to get the associated exponents). The values obtained from those correlations, shown in Table 2, are quite in agreement with their observed analogs. In practice, those relationships are crucial to estimate B_{\star} and \dot{M} , since an inaccuracy in the determination of L_X would lead to an erroneous value of the mass-loss rate through the $\dot{M} - F_X$ correlation.

All those considerations allow us to estimate the stellar magnetic field and the mass loss with our formalism. We illustrate those predictions by the blue bands in Figure 7. Note that without further assumption, our model predicts a broad range of possible B_{\star} (panel A) and \dot{M} (panel B) values. Since we are performing a systematic study of ϵ Eridani, we will first assume that the star follows the observational trends inferred from ZDI studies. Only the exponents situated in the light grey area defined in Figure 7 will be considered ($1 \leq p_B \leq 1.65$). A modification of the $B_{\star} - Ro$ relationship then corresponds to an horizontal shift in Figure 7. A change of normalization between $B_{\odot} = 0.6$ G (dashed blue line in Figure 7) and $B_{\odot} = 4$ G (dotted blue line in Figure 7), linked to the scatter in the ZDI studies dataset, results in a vertical shift in Figure 7. Browsing this parameter space then gives $3 \leq B_{\star} [G] \leq 47$ and $1.9 \times 10^{-14} \leq \dot{M} [M_{\odot}.\text{yr}^{-1}] \leq 1.2 \times 10^{-12}$.

The large-scale magnetic field of the star has been monitored for almost seven years, between January 2007 and October 2013, by Jeffers et al. (2014). We only consider the dipolar component of their ZDI maps, leading to field values between 6.15 and 19.8 G (See et al. 2017), thus constraining our estimates of the magnetic field (see the red band at the top of Figure 7). Taking into account those observations, we can con-

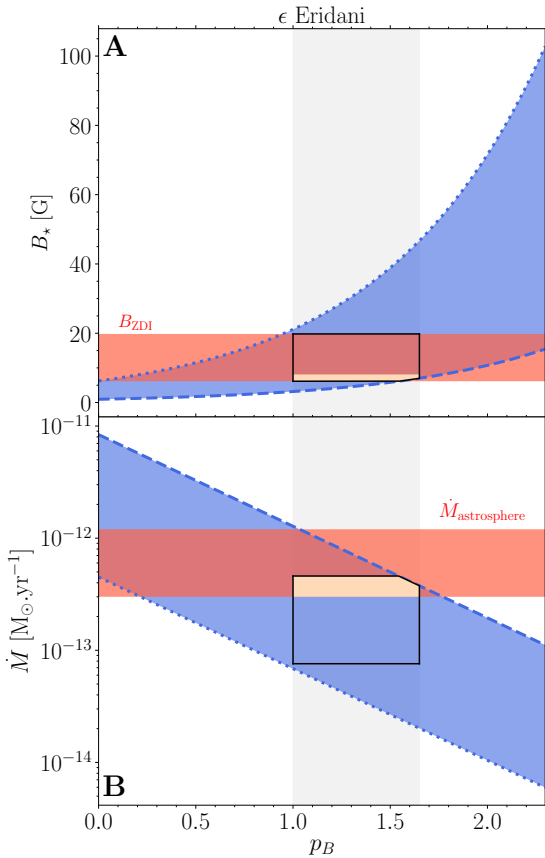


Fig. 7. Panel A: estimate of B_\star for ϵ Eridani as a function of p_B . Panel B: estimate of \dot{M} as a function of p_B . In blue: predictions of our prescriptions. Dashed blue lines: normalizations corresponding to $B_\odot = 0.6$ G. Dotted blue lines: normalizations corresponding to $B_\odot = 4$ G. Red bands: observational constraints on the dipolar component of the magnetic field (Jeffers et al. 2014; See et al. 2017) and the mass-loss rate (Wood et al. 2002). The light grey band corresponds to the upper and lower bounds of p_B from large sample of ZDI studies. The black contours delimit the region of B_\star and \dot{M} consistent with statistical ZDI studies and individual measurements of the large-scale magnetic field. In beige: estimates consistent with all the constraints considered.

strain the normalization factors and derive a narrower range for \dot{M} : $7.59 \times 10^{-14} \leq \dot{M} [M_\odot \text{yr}^{-1}] \leq 4.59 \times 10^{-13}$ (see the black contours in panel B of Figure 7).

Furthermore, Wood et al. (2002) measured the mass-loss rate of the star through its astrosphere’s Ly α absorption, leading to $\dot{M} \approx 6 \times 10^{-13} M_\odot \text{yr}^{-1}$. Uncertainties in the determination of this value, for instance in interstellar medium properties or wind variability, introduce a systematic error of 0.3 dex in $\log \dot{M}$, *i.e.* a factor of 2 in the mass-loss rate (see Wood et al. (2002) for more details). Therefore, we can assume a mass loss measured through ϵ Eridani’s astrosphere between $3 \times 10^{-13} M_\odot \text{yr}^{-1}$ and $1.2 \times 10^{-12} M_\odot \text{yr}^{-1}$ (see the red band in panel B of Figure 7). This constraint further refine the acceptable parameters of our model which leads to B_\star between 6.15 and 8 G (see the beige areas in Figure 7). It is worth noticing that our B_\star and \dot{M} prescriptions are consistent with both statistical approaches and individual measurements (as evident in the small beige areas). Furthermore, the wind of ϵ Eridani has been modelled in 3D with a MHD model by Alvarado-Gómez et al. (2016). They find a mass-loss ranging from 2.77×10^{-14} to $10.2 \times 10^{-14} M_\odot \text{yr}^{-1}$ for January 2010. Our approach is also compatible with these

values (see panel B in Figure 2).

The range of \dot{M} obtained (between 3×10^{-13} and $4.59 \times 10^{-13} M_\odot \text{yr}^{-1}$) allows us to estimate the coronal temperature T_c and the coronal density n_c for this particular star. Depending on the scenario considered (single density scaling, entropy equilibrium or single temperature scaling), since the normalization factor T_\odot has been fixed in Section 4.1.3, the range of p_B available provides directly upper and lower bounds of T_c with our prescriptions (see Table 1 and Appendix E for numerical values). The range of density is then determined by connecting the lower and upper bounds of \dot{M} and T_c . The corresponding numerical values for the coronal properties are shown in Table 3.

Table 3. Coronal properties of ϵ Eridani.

Scenario	T_c [MK]	n_c [10^8 cm^{-3}]
Single temperature scaling	2.83	0.34–0.52
Entropy equilibrium	1.73–1.85	3.53–3.46
Single density scaling	1.58–1.72	6.98–5.62

One can see that the entropy equilibrium scenario yields slightly higher temperatures compared to the single density scaling hypothesis, therefore resulting in lower densities for a given mass-loss rate. In the single temperature scaling scenario, T_c is independent of the B_\star and \dot{M} prescriptions because of the $T_l - F_X$ correlation (cf. equation (37)). Moreover, the star is here characterized by a low Rossby number in the unsaturated regime, leading to a higher coronal temperature than those derived from the two other scenarii. Hence, the coronal density, in the case of a single temperature scaling, reaches the lowest values in order to keep a consistent mass loss.

To sum up, we have shown with ϵ Eridani that it is possible to have an analytical prediction of the large-scale magnetic field and the mass-loss rate in agreement with all the observational constraints available, and to infer from the values obtained a range for the coronal properties of the star, according to different scenarii. Furthermore, with a systematic approach, relying on scaling laws and statistical considerations gives a quite large range for B_\star and \dot{M} , compared to well-constrained quantities coming from individual studies. In the case of ϵ Eridani, such a guess can deviate from the measured value by at most a factor 6 in B_\star and about one order of magnitude in \dot{M} . If for the study of an individual star, additional measurements are required to reduce the interval of confidence, we see how powerful our approach is to guess key trends along with stellar properties in an ensemble approach. Our formalism then provides a good estimate, given our minimal set of hypothesis, of the relevant quantities from general scaling laws and statistical trends, compatible with individual studies.

5. Conclusions and discussions

We have provided in this paper power-law prescriptions of all the relevant parameters required to describe consistently the spin-down of solar-type stars. We confirm that the magnetic field and the mass loss are involved in a one-to-one correspondence. This is the direct consequence of assuming a generic braking torque parametrization accounting for both the distribution of stellar rotation periods in open clusters and the Skumanich law in the unsaturated rotation regime. A mass loss-X-ray flux relation coming from astrospheres’ Ly α absorption (Wood et al. 2005), cou-

pled with the knowledge of the rotational dependency of the X-ray luminosity, allowed us to link the mass-radius dependency of the aforementioned quantities to their rotational dependency. This way, we have shown that a magnetic field depending on both the Rossby number and the stellar mass may be required to remain consistent with a whole suite of observational trends. Such an approach allows us to provide upper and lower bounds for the estimates of B_\star and \dot{M} as follows:

– Lower bound:

$$B_\star [G] = (0.6 - 4) \times \left(\frac{Ro}{Ro_\odot}\right)^{-1} \left(\frac{M_\star}{M_\odot}\right)^{-1.76} \quad (67)$$

$$\dot{M} [10^{-14} M_\odot \text{yr}^{-1}] = (0.79 - 14.7) \times \left(\frac{Ro}{Ro_\odot}\right)^{-2} \left(\frac{M_\star}{M_\odot}\right)^4 \quad (68)$$

– Upper bound:

$$B_\star [G] = (0.6 - 4) \times \left(\frac{Ro}{Ro_\odot}\right)^{-1.65} \left(\frac{M_\star}{M_\odot}\right)^{-1.04} \quad (69)$$

$$\dot{M} [10^{-14} M_\odot \text{yr}^{-1}] = (0.79 - 14.7) \times \left(\frac{Ro}{Ro_\odot}\right)^{-1} \left(\frac{M_\star}{M_\odot}\right)^{2.9} \quad (70)$$

Furthermore, given a simple polytropic wind model and an expression of the X-ray luminosity from radiative losses, we have been able to go back to the coronal properties by assuming different scenarii linking closed loops to coronal holes. This permits us to consider in a very simplified way magnetic geometry effects occurring in stellar atmospheres. Some of these scenarii (namely scenarii 2 and 3, see §3.5) allow us to reconcile temperature prescriptions deduced from X-ray emission and mass-loss rate constraints, hence providing a fully consistent framework. To demonstrate the usefulness of our study, we then applied it on a real star *e.g.* ϵ Eridani. We provided estimates of the magnetic field and the mass-loss rate consistent with the different observational constraints and gave a first assessment of its coronal properties. In a saturated rotation regime, we showed that a wind torque depending linearly on the rotation rate implies a magnetic field and a mass-loss rate independent of the Rossby number. We then found a similar behavior for the coronal temperature and density, depending on the physical scenario we adopted to connect open and closed regions.

We managed to infer all the exponents of our scaling laws from the $B_\star - Ro$ relation. Furthermore, in this paper we adopted an observational point of view to constrain the p_B exponent ($B_\star \propto Ro^{-p_B}$) by relying on the large sample of ZDI studies. One can also use theoretical dynamo scalings to determine the rotational dependency of the magnetic field (Augustson et al. 2017a). However, we have to bear in mind that those prescriptions are based on the magnetic energy content in the stellar interior over a wide spectral range while we considered in this work the large scale magnetic field at the stellar surface. To link the two approaches, one can fall back on a filling factor which may depend on stellar rotation (See et al. 2019).

Stellar metallicity has not been directly taken into account in our study. However, it could affect significantly the coronal density and the stellar mass loss (Suzuki 2018), thus influencing the wind braking torque. In our work, the effect of metallicity

on the stellar structure is included in the Rossby dependency. Therefore, studying the influence of metallicity on the rotational evolution of solar-type stars may be a promising avenue to test different torque prescriptions.

Furthermore, coronal temperature and density are directly linked to the choice of a wind model. In this work, to connect the mass-loss rate to the coronal properties we relied on an expression for \dot{M} valid in the case of a non-magnetized outflow of a pressure-driven polytropic wind. Considering a more realistic model such as a magnetized wind would introduce corrections in the mass loss expression due to the magnetocentrifugal effect (Preusse et al. 2005; Johnstone 2017), involving for instance the stellar rotation rate and the Alfvén radius. It may lead to implicit relations between the different prescriptions. Given that our formalism relies on the Matt et al. (2015) wind braking torque, which does not take into account such an effect, a pressure-driven hydrodynamic polytropic wind may be more suitable in this context to keep a consistent model. Modifications of the wind torque and the mass-loss rate may be required to deal with very fast rotators. More complex models could also be investigated, such as a polytropic gas with a spatially varying polytropic index (Johnstone et al. 2015a).

We have not considered in this paper a slow and a fast wind, which would be a way of improving even more our model. Indeed, for a pressure-driven wind, higher temperatures lead to faster winds. However, an anti-correlation is observed between the terminal speed of the two components of the solar wind and the coronal temperature of the source region, which may be due to a difference in the altitude of the heating region between the fast and the slow component (Geiss et al. 1995; Schwadron & McComas 2003). Therefore, more realistic wind acceleration processes, including the influence of coronal heating, have to be taken into account to deal with a fast and slow wind (Réville et al. 2019; Riley et al. 2019).

We have shown that the p_L exponent ($L_X \propto L_\star Ro^{-p_L}$) is one of the most important parameters allowing us to constrain efficiently all the different prescriptions, especially the B_\star and \dot{M} mass-radius dependency as well as the expression of the coronal properties. This way, an uncertainty on this exponent (Pizzolato et al. 2003; Wright et al. 2011) may lead to a significant scatter in our scaling laws. Therefore, our prescriptions could be significantly tightened if the interval of confidence of the p_L exponent could be reduced.

In the case of evolved stars, the decrease of the wind braking efficiency (van Saders et al. 2016) has not been studied in this work. However, the influence of this phenomenon on the different wind parameters and its eventual inconsistency with other observational constraints may be an application of our formalism. It could be possible to introduce a *re-saturation* regime at high Rossby numbers (Sadeghi Ardestani et al. 2017) and to look for hints of a breaking of gyrochronology in the physical quantities involved in stellar spin-down.

Acknowledgements. We would like to thank the anonymous referee and Sean Matt for helpful comments and suggestions regarding our work. The authors acknowledge funding from the European Union’s Horizon-2020 research and innovation programme (Grant Agreement no. 776403 Exoplanets-A). A.S. and A.S.B. acknowledge funding by ERC WHOLESUN 810218 grant, INSU/PNST, CNES-PLATO and CNES Solar Orbiter. A.S. acknowledges funding from the Programme National de Planétologie (PNP). This work benefited from discussions within the international team “The Solar and Stellar Wind Connection: Heating processes and angular momentum loss”, supported by the International Space Science Institute (ISSI). We also thank Victor Réville, Manuel Güdel, Colin Johnstone, Aurélie Astoul and Kyle Augustson for useful discussions.

References

- Agüeros, M. A., Covey, K. R., Lemonias, J. J., et al. 2011, *ApJ*, 740, 110
- Alvarado-Gómez, J. D., Hussain, G. A. J., Cohen, O. et al. 2016, *A&A* 594, A95
- Amard, L., Palacios, A., Charbonnel, C., et al. 2019, arXiv e-prints, arXiv:1905.08516
- Armitage, P. J. & Clarke, C. J. 1996, *MNRAS*, 280, 458
- Aschwanden M. J., 2004, *Physics of the Solar Corona. An Introduction*. Praxis Publishing Ltd; Chichester, UK
- Augustson, K., Mathis, S., & Brun, A. S. 2017a, ArXiv e-prints [arXiv:1701.02582]
- Barnes, S. A. 2003, *ApJ*, 586, 464
- Barnes, S. & Sofia, S. 1996, *ApJ*, 462, 746
- Benbakoura, M., Réville, V., Brun, A. S., Le Poncin-Lafitte, C., & Mathis, S. 2019, *A&A*, 621, A124
- Blackman E. G. & Owen J. E., 2016, *MNRAS*, 458, 1548
- Bouvier, J., Forestini, M., & Allain, S. 1997, *A&A*, 326, 1023
- Brandenburg, A., & Saar, S. H. 2000, in *ASP Conf. Ser. 198, Stellar Clusters and Associations: Convection, Rotation, and Dynamos*, ed. R. Pallavicini, G. Micela, & S. Sciortino (San Francisco, CA: ASP), 381
- Brun, A. S., Browning, M. K., Dikpati, M., Hotta, H., & Strugarek, A. 2015, *SSR*, 196, 101
- Brun, A. S., Miesch, M. S., & Toomre, J. 2004, *ApJ*, 614, 1073
- Brun, A. S., Strugarek, A., Varela, J., et al. 2017, *ApJ*, 836, 192
- Cranmer S. R., Gibson S. E. & Riley P., 2017, *SSR*, 212, 1345
- Cranmer, S. R. & Saar, S. H. 2011, *ApJ*, 741, 54
- Durney, B. R., & Latour, J. 1978, *Geophysical and Astrophysical Fluid Dynamics*, 9, 241
- Finley, A. J. & Matt, S. P. 2017, *ApJ*, 845, 46
- Finley, A. J. & Matt, S. P. 2018, *ApJ*, 854, 78
- Gallet, F. & Bouvier, J. 2015, *A&A*, 577, A98
- Garraffo, C., Drake, J. J., Cohen, O. 2016, *A&A*, 595, A110
- Garraffo, C., Drake, J. J., Dotte, A. et al. 2018, *ApJ*, 862, 90
- Geiss, J., Gloeckler, G., & von Steiger, R. 1995, *Space Science Review*, 72, 49
- Güdel, M. 2007, *Living Reviews in Solar Physics*, 4, 3
- Heyvaerts, J., & Priest, E. R. 1983, *A&A*, 117, 220
- Holzwarth, V., & Jardine, M. 2007, *A&A*, 463, 11
- Ivanova, N., & Taam, R. E. 2003, *ApJ*, 599, 516
- Jardine M. & Collier Cameron A., 2019, *MNRAS*, 482, 2853
- Jeffers, S. V., Petit, P., Marsden, S. C., Morin, J., Donati, J.-F., Folsom, C. P. and the BCooll collaboration 2014, *A&A*, 569, A79
- Johns-Krull, C. M. & Valenti, J. A. 2000, *Measurements of stellar magnetic fields*. In: Pallavicini R., Micela G., Sciortino S. (eds) *Stellar clusters and associations: convection, rotation, and dynamos*. *Astronomical Society of the Pacific, San Francisco, ASP conference series*, 198, 371
- Johnstone, C. P. 2017, *A&A*, 598, A24
- Johnstone, C. P., & Güdel, M. 2015, *A&A*, 578, A129
- Johnstone, C. P., Güdel, M., Lüftinger, T., Toth, G., & Brott, I. 2015a, *A&A*, 577, A27
- Johnstone, C. P., Güdel, M., Brott, I. & Lüftinger, T. 2015b, *A&A*, 577, A28
- Kawaler, S. D. 1988, *ApJ*, 333, 236
- Kippenhahn, R., & Weigert, A. 1994, *Stellar Structure and Evolution* (Berlin:Springer)
- Krishnamurthi, A., Pinsonneault, M. H., Barnes, S., & Sofia, S. 1997, *ApJ*, 480, 303
- Lamers, H. J. G. L. M., & Cassinelli, J. P. 1999, *Introduction to stellar winds*. Cambridge University Press; Cambridge, UK
- Landin, N. R., Mendes, L. T. S., & Vaz, L. P. R. 2010, *A&A*, 510, A46
- Lorenzo-Oliveira, D., Meléndez, J., Galarza, J. Y., et al. 2019, *MNRAS*, 485, L68
- Mathioudakis, M., Jess, D. B., & Erdélyi, R. 2013, *Space Sci. Rev.*, 175, 1
- McQuillan, A., Mazeh, T., & Aigrain, S. 2014, *ApJS*, 211, 24
- Matt, S. P., Brun, A.-S., Baraffe, I., Bouvier, J., & Chabrier, G. 2015, *ApJ*, 799, L23
- Matt, S. P., Pinzón, G., Greene, T. P., & Pudritz, R. E. 2012, *ApJ*, 745, 101
- Matt, S., & Pudritz, R. E. 2008, *ApJ*, 678, 1109
- Mestel, L., 1968, *MNRAS*, 138, 359.
- Mestel, L. & Spruit, H. C. 1987, *MNRAS*, 226, 57
- Montesinos, B., & Jordan, C. 1993, *MNRAS*, 264, 900
- Morel, P. & Lebreton, Y. 2008, *Ap&SS*, 316, 61
- Noyes, R. W., Weiss, N. O., & Vaughan, A. H. 1984, *ApJ*, 287, 769
- Ó Fionnagáin, D., & Vidotto, A. A. 2018, *MNRAS*, 476, 2465
- Parker, E. N. 1958, *ApJ*, 128, 664
- Petit, P., Dintrans, B., Aurière, M. et al. 2008 in SF2A-2014: SF2A-2008: Proceedings of the Annual meeting of the French Society of Astronomy and Astrophysics, 523, eds.: C. Charbonnel, F. Combes and R. Samadi.
- Pevtsov, A. A., Fisher, G. H., Acton, L. W., et al. 2003, *ApJ*, 598, 1387
- Pizzolato, N., Maggio, A., Micela, G., Sciortino, S., & Ventura, P. 2003, *A&A*, 397, 147
- Preibisch, T. 1997, *A&A*, 320, 525
- Preusse, S., Kopp, A., Büchner, J. & Motschmann, U. 2005, *A&A*, 434, 1191
- Reiners, A. 2012, *LRSP*, 9, 1
- Reiners, A. & Mohanty, S. 2012, *ApJ*, 746, 43
- Reiners, A., Schüssler, M., & Passegger, V. M. 2014, *ApJ*, 794, 144
- Réville, V., Brun, A.-S., Matt, S. P., Strugarek, A., & Pinto, R. F. 2015a, *ApJ*, 798, 116
- Réville, V., Brun, A.-S., Strugarek, A., et al. 2015b, *ApJ*, 814, 99
- Réville, V., Folsom, C. P., Strugarek, A., & Brun, A. S. 2016, *ApJ*, 832, 145
- Réville, V., Tenerani, A. & Velli, M. 2018, *ApJ*, 866, 38
- Réville, V., Velli, M., Panasenco, O. et al. 2019 (in press.). *The role of Alfvén waves dynamics on the large scale properties of the solar wind: comparing a MHD simulation with PSP E1 data*.
- Riley, P., Linker, J. A., Mikic, Z. et al. 2019, *ApJ*, 884, 18
- Rosner, R., Tucker, W.H., & Vaiana, G.S. 1978a, *ApJ* 220, 643
- Sadeghi Ardestani, L., Guillot, T., & Morel, P. 2017, *MNRAS*, 472, 2590
- Sakurai, T. 1985, *A&A*, 152, 121
- Saumon, D., Hubbard, W. B., Burrows, A., Guillot, T., Lunine, J. I., Chabrier, G., 1996, *ApJ*, 460, 993
- Schatzman, E. 1962, *AnAp*, 25, 18
- Schwadron, N. A. & McComas, D. J. 2003, *ApJ*, 599, 1395
- See, V., Jardine, M., Vidotto, A. A., et al. 2014, *A&A*, 570, A99
- See, V., Jardine, M., Vidotto, A. A., et al. 2017, *MNRAS*, 466, 1542
- See, V., Matt, S. P., Folsom, C. P. et al. 2019, *ApJ*, 876, 118
- Skumanich, A. 1972, *ApJ*, 171, 565
- Skumanich, A. 2019, *ApJ*, 878, 35
- Suzuki, T. K. 2018, *PASJ*, 70, 34
- Suzuki T. K., Imada S., Kataoka R., Kato Y., Matsumoto T., Miyahara H. & Tsuneta S., 2013, *PASJ*, 65, 98
- Suzuki, T. K. & Inutsuka, S. 2006, *JGR*, 111, A06101
- Tu L., Johnstone C. P., Güdel M., Lammer H., 2015, *A&A*, 577, L3
- Velli, M., Grappin, R., & Mangeney, A. 1989, *PhRvL*, 63, 1807
- Vidotto, A. A. & Bourrier, V. 2017, *MNRAS*, 470, 4026
- Vidotto, A. A., Gregory, S. G., Jardine, M., et al. 2014, *MNRAS*, 441, 2361
- Weber, E. J., & Davis, Jr., L. 1967, *ApJ*, 148, 217
- Wedemeyer-Böhm, S., Lagg, A., Nordlund, A. 2009, *Space Sci. Rev.*, 144, 317
- Wright, N. J., Drake, J. J., Mamajek, E. E., & Henry, G. W. 2011, *ApJ*, 743, 48
- van Saders, J. L., Ceillier, T., Metcalfe, T. S., et al. 2016, *Nature*, 529, 181
- Wood, B. E., Müller, H.-R., Zank, G. P., & Linsky, J. L. 2002, *ApJ*, 574, 412
- Wood, B. E., Müller, H.-R., Zank, G. P., Linsky, J. L., & Redfield, S. 2005, *ApJ Letters*, 628, L143
- Wood, B. E., Laming, J. M., Warren, H. P., & Poppenhaeger, K. 2018, *ApJ*, 862, 66
- Zhang, M., & Penev, K. 2014, *ApJ*, 787, 131 A124

Appendix A: Mass loss for a Parker polytropic wind

The goal of this section is to compute the stellar mass loss by assuming a radial polytropic pressure-driven outflow, with an index γ . We will follow Lamers & Cassinelli (1999) in the remainder of this section. The wind accelerates with distance and its velocity v reaches the speed of sound c_s at a critical radius $r_c = GM_\star/2c_s^2(r_c)$ (Parker 1958). The momentum equation leads to the following integral formulation:

$$e_\gamma = \frac{v^2}{2} + \frac{c_s^2}{\gamma-1} - \frac{GM_\star}{r} = C^{\text{te}}. \quad (\text{A.1})$$

Such a constant can be estimated at the critical radius as follows:

$$e_\gamma = \frac{5-3\gamma}{\gamma-1} \frac{GM_\star}{4r_c}. \quad (\text{A.2})$$

Furthermore, from the mass conservation, we know that $\rho v r^2$, with ρ the density of the wind, is a constant. As $c_s^2 \propto \rho^{\gamma-1}$ for a polytrope, the speed of sound obeys to the following expression:

$$\frac{c_s^2}{c_s^2(r_c)} \propto \left(\frac{v}{c_s(r_c)}\right)^{1-\gamma} \left(\frac{r}{r_c}\right)^{2-2\gamma}. \quad (\text{A.3})$$

By defining $w = v/c_s(r_c)$ and $x = r/r_c$, equation (A.1) becomes:

$$w^{\gamma+1} - w^{\gamma-1} \left(\frac{4}{x} + \frac{5-3\gamma}{\gamma-1}\right) + \frac{2}{\gamma-1} x^{2-2\gamma} = 0. \quad (\text{A.4})$$

By definition of the critical radius, we have:

$$c_s^2(r_c) = \frac{GM_\star}{2r_c} = \Lambda x_0 c_s^2(R_\star), \quad (\text{A.5})$$

where $x_0 = R_\star/r_c$ and $\Lambda = v_{esc}^2/4c_s^2(R_\star)$. Therefore, thanks to equation (A.3), assessing equation (A.4) at the base of the corona, which is assumed to be situated approximately at the stellar radius, gives the following relationship:

$$\left(\Lambda x_0^{3-2\gamma}\right)^{\frac{\gamma+1}{\gamma-1}} - \left(\Lambda x_0^{3-2\gamma}\right) \left(\frac{4}{x_0} + \frac{5-3\gamma}{\gamma-1}\right) + \frac{2}{\gamma-1} x_0^{2-2\gamma} = 0. \quad (\text{A.6})$$

If we assume that $c_s^2(R_\star) \ll v_{esc}^2$, i.e. $x_0 \ll 1$ and $\Lambda \gg 1$, we find by neglecting the first term in equation (A.6) :

$$x_0 = \frac{2-4(\gamma-1)\Lambda}{(5-3\gamma)\Lambda}. \quad (\text{A.7})$$

At the base of the corona, we can assume that $w \ll 1$. Therefore, equation (A.4) becomes, by neglecting the first term:

$$w(R_\star) = \left[\frac{2}{\gamma-1} x_0^{3-2\gamma} \left(4 + \frac{5-3\gamma}{\gamma-1} x_0\right)^{-1} \right]^{\frac{1}{\gamma-1}} = \Lambda^{\frac{1}{\gamma-1}} x_0^{\frac{3-2\gamma}{\gamma-1}}. \quad (\text{A.8})$$

Then the wind speed at the same distance can be expressed as:

$$v(R_\star) = c_s(r_c)w(R_\star) = c_s(R_\star)w(R_\star)^{\frac{\gamma+1}{2}} x_0^{\gamma-1}. \quad (\text{A.9})$$

It is now possible to estimate the mass loss as follows:

$$\begin{aligned} \dot{M} &= 4\pi\rho(R_\star)R_\star^2 v(R_\star) \\ &= 2\pi m_p n_c R_\star^2 c_s(R_\star) \Lambda^{\frac{\gamma+1}{2}} x_0^{\frac{5-3\gamma}{2(\gamma-1)}}. \end{aligned} \quad (\text{A.10})$$

As $c_s(R_\star) = \sqrt{2\gamma k_B T_c/m_p}$ for a fully ionized wind, the mass loss has the following dependencies:

$$\dot{M} \propto \left(\frac{M_\star}{M_\odot}\right)^2 \left(\frac{n_c}{n_\odot}\right) \left(\frac{T_c}{T_\odot}\right)^{-\frac{3}{2}} \left[1 - \frac{T_{\min,\odot}}{T_\odot} \frac{M_\star R_\odot T_\odot}{M_\odot R_\star T_c}\right]^{\frac{5-3\gamma}{2(\gamma-1)}}, \quad (\text{A.11})$$

with $T_{\min,\odot} = (1-1/\gamma) G m_p M_\odot / 2k_B R_\odot \approx 11 \times 10^6 (1-1/\gamma)$ K.

Appendix B: X-ray luminosity from radiative losses

The goal of this section is to compute the X-ray luminosity of the star from coronal properties. If we assume that the corona is fully ionized and optically thin, the X-ray luminosity emitted by a volume of electrons through free-free radiation can be expressed as (Aschwanden 2004; See et al. 2014):

$$L_X = \Lambda(\bar{T}_l) \int_{\text{dead zone}} n_l^2 dV \propto \Lambda(\bar{T}_l) \bar{n}_l^2 R_\star^3 \left(\frac{r_{dz}^3}{R_\star^3} - 1\right), \quad (\text{B.1})$$

where \bar{T}_l and \bar{n}_l are respectively the mean temperature and the mean density in the dead zone, r_{dz} is the radius of the dead zone and $\Lambda(\bar{T}_l)$ is the radiative loss function (Rosner, Tucker & Viana 1978a; Aschwanden 2004; Blackman & Owen 2016), estimated as:

$$\Lambda(\bar{T}_l) [\text{erg cm}^3 \text{ s}^{-1}] = 10^{-17.73} \bar{T}_l^{-\frac{2}{3}}. \quad (\text{B.2})$$

This prescription is assumed to be accurate for $\bar{T}_l \approx 2-10$ MK and acceptable as an average down to 0.4 MK.

To estimate the radius of the dead zone, we assume a dipolar magnetic field in the closed-field region, where the pressure gradient and the centrifugal force are not strong enough to distort the field lines. The closed loops then trap hot gas and prevent the flow of a stellar wind, allowing us to neglect the ram pressure of the gas in this area. The edge of the dead zone is here assimilated to a limit of confinement of the plasma and therefore can be estimated with the following pressure equilibrium:

$$p_{th}(r_{dz}) = p_{mag}(r_{dz}), \quad (\text{B.3})$$

where $p_{th}(r_{dz})$, $p_{mag}(r_{dz})$ are respectively the thermal and the magnetic pressures of the gas estimated at the edge of the dead zone. Since we consider a dipolar magnetic field, equation (B.3) becomes:

$$p_{th}(r_{dz}) = \frac{B_\star^2}{2\mu_0} \left(\frac{R_\star}{r_{dz}}\right)^6. \quad (\text{B.4})$$

If we consider that the dead zone is filled with an ideal gas of constant temperature $\bar{T}_l = T_l$ and a density at the edge of the dead zone evolving similarly to the density at the base of the corona n_l , i.e. $n_l(r_{dz}) = K n_l$, with K a constant independent of any stellar parameter, then $p_{th}(r_{dz}) = n_l(r_{dz}) k_B T_l = K n_l k_B T_l$. The radius of the dead zone then becomes:

$$\frac{r_{dz}}{R_\star} = \frac{r_{dz,\odot}}{R_\odot} \left(\frac{B_\star}{B_\odot}\right)^{\frac{1}{3}} \left(\frac{n_l}{n_{l,\odot}}\right)^{-\frac{1}{6}} \left(\frac{T_l}{T_{l,\odot}}\right)^{-\frac{1}{6}}, \quad (\text{B.5})$$

where:

$$\frac{r_{dz,\odot}}{R_\odot} = \left(\frac{1}{K} \frac{B_\odot^2}{2\mu_0 k_B n_{l,\odot} T_{l,\odot}}\right)^{\frac{1}{6}}. \quad (\text{B.6})$$

If we assume that \bar{n}_l varies the same way as the density at the base of the corona, we can express the X-ray luminosity as a function of more explicit stellar parameters:

$$L_X \propto \left(\frac{T_\odot}{T_l}\right)^{\frac{2}{3}} \left(\frac{n_l}{n_{l,\odot}}\right)^2 \left(\frac{R_\star}{R_\odot}\right)^3 \left[\left(\frac{r_{dz,\odot}}{R_\odot}\right)^3 \left(\frac{B_\star}{B_\odot}\right) \left(\frac{n_{l,\odot}}{n_l}\right)^{\frac{1}{2}} \left(\frac{T_{l,\odot}}{T_l}\right)^{\frac{1}{2}} - 1\right] \quad (\text{B.7})$$

By assuming $r_{dz}^3/R_\star^3 \gg 1$, the X-ray luminosity becomes:

$$L_X \propto \left(\frac{R_\star}{R_\odot}\right)^3 \left(\frac{B_\star}{B_\odot}\right) \left(\frac{n_l}{n_{l,\odot}}\right)^{\frac{3}{2}} \left(\frac{T_l}{T_{l,\odot}}\right)^{-\frac{7}{6}}. \quad (\text{B.8})$$

Appendix C: Conditions on the coronal temperature to generate a transsonic wind

The goal of this section is to investigate the consequences of the positiveness of the mass-loss rate on the coronal temperature. We will assume in coronal holes a correlation between the X-ray flux and the coronal temperature T_c like in the closed loops case

$$T_c \propto F_X^j, \quad (\text{C.1})$$

where the exponent j , different from j_l because of the possible difference of heating efficiency between open-field and closed-field regions, has to be determined. As for T_l , we can express T_c as a function of the Rossby number and the stellar mass

$$T_c \propto Ro^{-p_L j} M_\star^{(\eta-2\xi)j}, \quad (\text{C.2})$$

which leads to constraints similar to those obtained in §3.2, namely

$$p_T = p_L j, \quad (\text{C.3})$$

$$\xi r_T + m_T = (\eta - 2\xi)j. \quad (\text{C.4})$$

By eliminating the j exponent, the combined mass-radius dependency of T_c can be inferred from its Rossby dependency with

$$\xi r_T + m_T = \frac{\eta - 2\xi}{p_L} p_T. \quad (\text{C.5})$$

In the case of a pressure-driven radial polytropic wind, the coronal temperature has to be greater than a threshold value to keep a positive mass-loss rate, according to equation (10):

$$\frac{T_c}{T_\odot} \frac{R_\star}{R_\odot} \frac{M_\odot}{M_\star} > \frac{T_{\min,\odot}}{T_\odot}, \quad (\text{C.6})$$

which with equation (41) gives

$$\left(\frac{Ro}{Ro_\odot}\right)^{-p_T} \left(\frac{M_\star}{M_\odot}\right)^{\xi(r_T+1)+m_T-1} > \frac{T_{\min,\odot}}{T_\odot}. \quad (\text{C.7})$$

We consider here stars with $0.5M_\odot \leq M_\star \leq 1.4M_\odot$ (corresponding to F, G and K spectral types) and a Rossby number lesser than $10 Ro_\odot$. In order to keep a well-defined mass-loss rate for all those stars, it is necessary to fulfill the following condition:

$$10^{-p_T} m_{\text{lim}}^{\xi(r_T+1)+m_T-1} > \frac{T_{\min,\odot}}{T_\odot}, \quad (\text{C.8})$$

where m_{lim} is equal to 0.5 if $\xi(r_T + 1) + m_T - 1 > 0$ and 1.4 otherwise. This will define a maximal value for the p_T exponent, considering the range of stellar masses and Rossby numbers considered:

$$p_T < \frac{(\xi - 1) \log_{10}(m_{\text{lim}}) - \log_{10}\left(\frac{T_{\min,\odot}}{T_\odot}\right)}{1 - \frac{\eta-2\xi}{p_L} \log_{10}(m_{\text{lim}})} \equiv p_{T,\text{max}}. \quad (\text{C.9})$$

This maximal p_T is shown in Figure C.1. One can notice that $p_{T,\text{max}}$ decreases with the adiabatic index γ because the minimal temperature required to generate a transsonic wind increases with γ . The $p_{T,\text{max}}$ exponent then vanishes at a certain value of γ , beyond which it is not possible to obtain a consistent power-law prescription of T_c without changing the value of T_\odot .

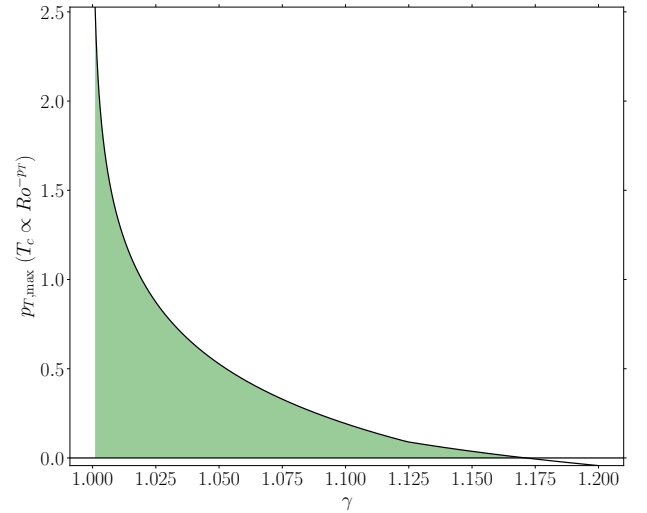


Fig. C.1. Maximal value of p_T needed to keep a positive mass-loss rate, as a function of the adiabatic index γ , for $\eta = 4$, $\xi = 0.9$, $p_L = 2$, $T_\odot = 1.5$ MK. In green: consistent values of p_T .

Appendix D: Power-law expression of the coronal density from wind model considerations

For a pressure-driven polytropic wind, the coronal density n_c can be inferred from the mass-loss rate as

$$n_c \propto Ro^{-p_M} R_\star^{r_M} M_\star^{m_M-2} T_c^{\frac{3}{2}} \left[1 - \frac{T_{\min,\odot}}{T_\odot} \frac{M_\star}{M_\odot} \frac{R_\odot}{R_\star} \frac{T_\odot}{T_c}\right]^{\frac{3\gamma-5}{2(\gamma-1)}}. \quad (\text{D.1})$$

In order to simplify this expression, we define $X = \frac{M_\star}{M_\odot} \frac{R_\odot}{R_\star} \frac{T_\odot}{T_c}$ and

$$Q(X) = \left[1 - \frac{T_{\min,\odot}}{T_\odot} X\right]^{\frac{3\gamma-5}{2(\gamma-1)}}. \quad (\text{D.2})$$

To approximate this function by a power law, which can be motivated by the n_l prescription for instance, we introduce the quantity

$$F(\gamma, X) = \frac{\partial[\ln Q(X)]}{\partial[\ln X]}. \quad (\text{D.3})$$

The expression of the function Q then gives

$$F(\gamma, X) = \frac{3\gamma - 5}{2(\gamma - 1)} \frac{\partial[\ln(1 - \frac{T_{\min,\odot}}{T_\odot} X)]}{\partial[\ln X]}. \quad (\text{D.4})$$

During the Main Sequence, if we assume a stellar radius approximately proportional to the mass of the star, *i.e.* $\xi \approx 1$, we can consider that $M_\star R_\odot / M_\odot R_\star \approx 1$. Furthermore, for small values of p_T (and small values of $\xi r_T + m_T$ through the $T_c - F_X$ correlation), which is required to generate a transsonic polytropic wind, we can assume that the coronal temperature presents only small variations for the stellar parameters we consider, leading to $T_c / T_\odot \approx 1$ in $F(\gamma, X)$. This way, $X \approx 1$ and

$$F(\gamma, X) \approx \frac{5 - 3\gamma}{2(\gamma - 1)} \frac{T_{\min,\odot} / T_\odot}{1 - T_{\min,\odot} / T_\odot} \equiv F(\gamma). \quad (\text{D.5})$$

We can therefore express the coronal density as

$$n_c \propto \left(\frac{Ro}{Ro_\odot}\right)^{-p_n} \left(\frac{R_\star}{R_\odot}\right)^{r_n} \left(\frac{M_\star}{M_\odot}\right)^{m_n}, \quad (\text{D.6})$$

with

$$p_n = p_{\dot{M}} + \left(\frac{3}{2} - F(\gamma) \right) p_T, \quad (\text{D.7})$$

$$r_n = r_{\dot{M}} + \frac{3}{2} r_T - F(\gamma)(1 + r_T), \quad (\text{D.8})$$

$$m_n = m_{\dot{M}} - 2 + \frac{3}{2} m_T - F(\gamma)(m_T - 1). \quad (\text{D.9})$$

Appendix E: Exponents for other scenarii

Table E.1. Parameters defining the Γ_{wind} , B_* , \dot{M} , T_c & n_c prescriptions for $p_B = 1$ and $p_B = 1.65$ in the single temperature scaling scenario and the entropy equilibrium scenario

Lower bound	Upper bound	Equation
<i>Free parameters.</i>		
$\gamma = 1.05^a$	-	(10)
$m = 0.2177^d$	-	(6)
<i>Constrained parameters.</i>		
$T_{\odot} = 1.5 \text{ MK}^a$	-	(10)
$\eta = 4^b$, $\xi = 0.9^b$	-	(12), (13)
$p_L = 2^c$	-	(24)
$a = 3.1^e$, $b = 0.5^e$	-	(15)
$p_B = 1$	$p_B = 1.65^f$	(7)
$\xi r_B + m_B = -1.76$	$\xi r_B + m_B = -1.04$	(7)
$p_{\dot{M}} = 2$	$p_{\dot{M}} = 1$	(9)
$\xi r_{\dot{M}} + m_{\dot{M}} = 4$	$\xi r_{\dot{M}} + m_{\dot{M}} = 2.9$	(9)
$w = 1$	$w = 0.5$	(23)
<i>Single temperature scaling.</i>		
$p_T = 0.52$	-	(48)
$\xi r_T + m_T = 0.57$	-	(49)
$j = 0.26$	-	(C.1)
<i>Entropy equilibrium.</i>		
$p_T = 0.17$	$p_T = 0.11$	(53)
$\xi r_T + m_T = 0.19$	$\xi r_T + m_T = 0.13$	(55)
$j = 0.09$	$j = 0.055$	(C.1)
$p_n = 0.55$	$p_n = 0.03$	(54)
$\xi r_n + m_n = 1.40$	$\xi r_n + m_n = 0.83$	(56)

^(a) Réville et al. (2015b) ^(b) Kippenhahn & Weigert (1994)

^(c) Pizzolato et al. (2003) ^(d) Matt et al. (2012) ^(e) Matt et al. (2015) ^(f) See et al. (2017)

Appendix F: Observational trends used in this work and their caveats

Table F.1. Observational trends used in this work and their caveats

Ingredient	References	Caveats
Skumanich law	Skumanich (1972) Gallet & Bouvier (2015) van Saders et al. (2016)	Uncertainty in the core-envelope coupling timescale dependency. Possible break of gyrochronology for evolved stars.
Wind braking torque	Matt et al. (2015)	Slows rotators with lower stellar masses spinning too fast compared to the one observed in the <i>Kepler</i> field. Possible dependency on the metallicity.
$L_X - Ro$ relationship	Pizzolato et al. (2003) Wright et al. (2011) Reiners et al. (2014)	Uncertainties in the trend obtained due to observational biases.
ZDI studies	Reiners (2012) Vidotto et al. (2014) See et al. (2017)	Only large-scale unsigned magnetic flux can be measured, missing small-scale field, observational uncertainties.
Astrospheric wind measurements	Wood et al. (2002, 2005)	Assumed interstellar medium parameters, limited number of systems, large scatter in scaling law.